DIAGENETIC SMECTITE-TO-ILLITE TRANSITION IN CLAY-RICH SEDIMENTS: A REAPPRAISAL OF X-RAY DIFFRACTION RESULTS USING THE MULTI-SPECIMEN METHOD

BRUNO LANSON*[†], BORIS A. SAKHAROV**, FRANCIS CLARET*,***
and VICTOR A. DRITS**

ABSTRACT. Smectite illitization is a common mineralogical reaction occurring during the burial diagenesis of clay-rich sediments and shales, and has thus attracted sustained interest over the last fifty years. Prior studies have concluded that smectite illitization proceeds through a steady set of homogeneous reactions involving intermediate mixed layers of varying compositions. In these intermediate structures, illite and smectite or, more generally, expandable layers (I and Exp layers, respectively) coexist among the same crystallites giving rise to non-periodic structures (I-Exp) characterized by specific diffraction effects. Consistent with this model, reaction progress was characterized by the simultaneous increase in the illite content in I-Exp and in their stacking order leading to the following mineralogical sequence: smectite → randomly interstratified I-Exp with high smectite contents (> 50% Exp layers) → ordered I-Exp with high illite contents (> 50% I layers) → illite. Although reaction mechanisms have been extensively debated, this structural characterization has not been challenged, possibly due to a methodological bias. In the present study, X-ray diffraction patterns typical of the diagenetic illitization of smectite are interpreted using modern approaches involving profile fitting (multi-specimen method). Novel insights into the structure of intermediate reaction products are thus obtained. In particular, original clay parageneses are described that include the systematic presence of illite, kaolinite, chlorite and a mixed layer containing kaolinite and expandable layers (K-Exp).

In contrast to previous descriptions, the early stages of smectite illitization are characterized by the coexistence of discrete smectite and of a randomly interstratified I-Exp with a high content of illite layers (>50% I layers). Both the smectite and the I-Exp are authigenic and form under shallow burial, that is at low temperature conditions. With increasing burial depth, the relative proportion of I-Exp increases, essentially at the expense of discrete smectite, and the composition of I-Exp becomes slightly more illitic. In the second stage of smectite illitization, two illite-containing mixed layers are observed. They result from two parallel reaction mechanisms affecting the randomly interstratified I-Exp present in the shallow section of the series. The first reaction implies the dissolution of this randomly interstratified I-Exp and leads to the crystallization of an ordered I-Exp without significant illitization, possibly because of the low K-availability. The second reaction affecting the randomly interstratified I-Exp implies the growth of trioctahedral (Mg, Al) hydroxide sheets in Exp interlayers, thus developing di-trioctahedral chlorite layers (Ch layers) in the initial I-Exp to form an I-Exp-Ch. A layer-by-layer mechanism is hypothesized for this reaction. In this scheme, Mg cations released by the dissolution-recrystallization reaction of I-Exp likely represent the source of Mg for the formation of brucite-like sheets in expandable interlayers, and thus of the I-Exp-Ch.

The reported structural characterization of smectite illitization intermediate products contradicts the conventional wisdom of a homogeneous reaction through a series of pure mixed layers of variable composition. In contrast, the coexistence of different phases implies a heterogeneous reaction via a sequence of intermediate phases and requires reassessing the reaction mechanisms proposed in the literature. The compositional range (relative proportion of the different layer types) of these

* Mineralogy and Environments Group, LGCA, Maison des Géosciences, BP53, Université Joseph Fourier—CNRS, 38041 Grenoble Cedex 9, France
** Geological Institute, Russian Academy of Sciences, 7 Pyzhevsky street, 119017 Moscow, Russia
*** BRGM, 3 av. Claude Guillemin, F-45060 Orléans cedex 2, France
† Corresponding author: bruno.lanson@obs.uf-grenoble.fr

phases is limited and smectite illitization proceeds essentially as relative proportions of the different phases vary. In addition, reaction kinetics and stability of the different intermediate products also need to be reconsidered.

Key words: Clay minerals, Clay diagenesis, Illite-smectite, Mixed-layering, interstratification, XRD, Gulf Coast, Smectite illitization.

<div align="center">INTRODUCTION</div>

For about half a century, smectite illitization has been extensively described in different geological contexts: burial diagenesis of clay-rich sediments (Burst, 1957, 1969; Weaver, 1957, 1959; Perry and Hower, 1970; Hower and others, 1976; Srodon, 1978, 1984a; Boles and Francks, 1979; Velde and others, 1986; among many others), hydrothermal alteration of volcanic tuffs (Inoue and others, 1978, 1988, 2005; Inoue and Utada, 1983; Altaner and others, 2003), metasomatic alteration of bentonites (Hoffman and Hower, 1979; Velde and Brusewitz, 1982, 1986; Inoue and others, 1990; Sucha and others, 1993; Li and others, 1997), and contact metamorphism (Nadeau and Reynolds, 1981; Pytte and Reynolds, 1989; Drits and others, 2007). Although different reaction mechanisms have been inferred (see Altaner and Ylagan, 1997, for a review; Srodon and others, 2000), this mineralogical transition has been systematically described to occur through mixed layers. In these intermediate structures, illite and smectite or, more generally, expandable layers (I and Exp layers, respectively) coexist among the same crystallites giving rise to non-periodic structures, hereafter referred to as I-Exp. The structural characterization of I-Exp, essential for the reconstruction of thermal and chemical paleoconditions, requires determining the nature of interstratified layers, their relative proportions and their stacking sequences through analysis of their specific diffraction effects (see Reynolds, 1980; Drits and Tchoubar, 1990; Moore and Reynolds, 1997, for details). Such analysis has revealed that smectite illitization is a continuous two-stage reaction characterized by a steady increase of the illite content in I-Exp and by the simultaneous increase of stacking order: illite and expandable layers are interstratified at random when expandable layers dominate ("R0 zone"—early diagenesis), whereas interstratification is ordered when illite prevails ("R ≥ 1 zone"—late-stage diagenesis; Shutov and others, 1969; Perry and Hower, 1970, 1972; Hower and others, 1976; Bethke and others, 1986; Srodon, 1999).

Following these pioneering works, simplified methods have been proposed for the structural characterization of I-Exp from X-ray diffraction (XRD) data (Srodon, 1980, 1981, 1984b; Watanabe, 1981, 1988; Velde and others, 1986; Inoue and others, 1989; Moore and Reynolds, 1997). These methods essentially rely on peak migration curves which link the position of a given reflection (or of a set of reflections) to the composition (relative proportion of the different layer types) of the mixed layers and to their stacking order. Peak migration curves were obtained mostly from XRD patterns calculated using programs implemented from Reynolds (1967, 1980) or Watanabe (1981) algorithms. These calculations were essentially restricted to I-Exp composition and ordering that were described in the early works reported above, thus confining the simplified identification methods to these specific mixed layers. Logically, the early description of smectite illitization was not challenged by the numerous subsequent case studies. The lack of direct comparison between experimental and calculated XRD patterns concealed possible incomplete or erroneous identifications. A significant proportion of the studies devoted to smectite illitization thus focused on the definition of reaction mechanisms and on the possible use of this mineralogical transformation as a paleogeothermometer. For the latter purpose, the influence of time and temperature (Hower and others, 1976; Velde and Vasseur, 1992), K availability (Huang, 1993; Bauer and Velde, 1999), and water/rock ratio (Whitney, 1990) on reaction progress was estimated.

However, a more appropriate crystallography-based approach has been developed over the last decade. In particular, direct comparison between calculated and experimental diffraction patterns has been favored and has allowed reproduction of not only the positions of the reflections but also of their profiles, both of which are strongly influenced by interstratification. In addition to the frequent occurrence of multi-component mixed layers in nature, the multi-specimen method proposed initially by Drits and others (1997a), and by Sakharov and others (1999a, 1999b) uncovered the existence of mixed layers exhibiting "unusual" composition and/or stacking order (Drits and others, 1997a, 2002a, 2002b, 2004, 2007; Sakharov and others, 1999b, 2004; Lindgreen and others, 2000, 2002; Claret and others, 2004; McCarty and others, 2004). This new approach thus challenges the commonly accepted description of smectite illitization in diagenetic series by invalidating hypotheses sustaining usual I-Exp identification criteria such as homogeneity of the swelling behavior, random interstratification restricted to smectite-dominated mixed layers, absence of segregation and of partial ordering, *et cetera* (see Lanson, 2005, for further discussion).

The present study thus aims at obtaining an accurate structural characterization of samples characteristic of diagenetic smectite illitization in clay-rich sediments from the modeling of their XRD patterns. The proposed models are shown to be consistent with the coexistence of discrete smectite with I-Exp, as has been observed on similar samples with transmission electron microscopy. In addition, the definition of structure models at various stages of the reaction constrains the possible reaction mechanisms of this transformation. In particular, analysis of stacking parameters refutes the solid-state transformation hypothesis for illitization of I-Exp over the "R0 zone", and for the transition from randomly interstratified I-Exp to ordered varieties, consistent with crystal growth features reported during smectite illitization. It is shown also that part of the I-Exp formed early in the "R0 zone" transforms, possibly through solid-state processes, into a complex mixed layer present in the deeper samples.

MATERIALS AND METHODS

Samples

Samples were collected in two different onshore wells in the Texas Gulf Coast (Carter—Tyler County in central Gulf Coast Texas, and Mustang Island—Nueces County in south Gulf Coast Texas). These wells have been described previously by Velde and Espitalié (1989), and Velde and Vasseur (1992), and the stratigraphic age of the samples ranges from Cretaceous to Eocene (Carter well) and from Eocene to Pleistocene (Mustang Island). In the two wells, little or no erosion has occurred and present depths are approximately maximum burial depths. The temperature gradient is similar in both wells (32.7°C/km and 35°C/km, in Mustang Island and Carter, respectively), and they both extend through most of the smectite-to-illite transition (fig. 1).

Experimental

Carbonates were removed from all samples using the acetic acid-acetate buffer method described in Moore and Reynolds (1997). Then, organic matter was removed at 50°C by adding small aliquots of hydrogen peroxide (H_2O_2—30%) to the suspension until gaseous emission ceased. The <2 μm size fraction was extracted by centrifugation for a set of samples selected from −2170 to −5500 m in Carter and Mustang Island boreholes. From preliminary XRD results, 6 of the initial samples were selected as representative of the complete transition between "smectite-rich" and "illite-rich" samples in Gulf Coast series. All samples were selected in the Carter well at 2170, 3660, 4000, 4640, 5010, and 5180 m (samples A-F).

To minimize the contributions from mica, kaolinite, chlorite and quartz, the <0.2 μm size fraction was extracted for these 6 samples. This fraction was then
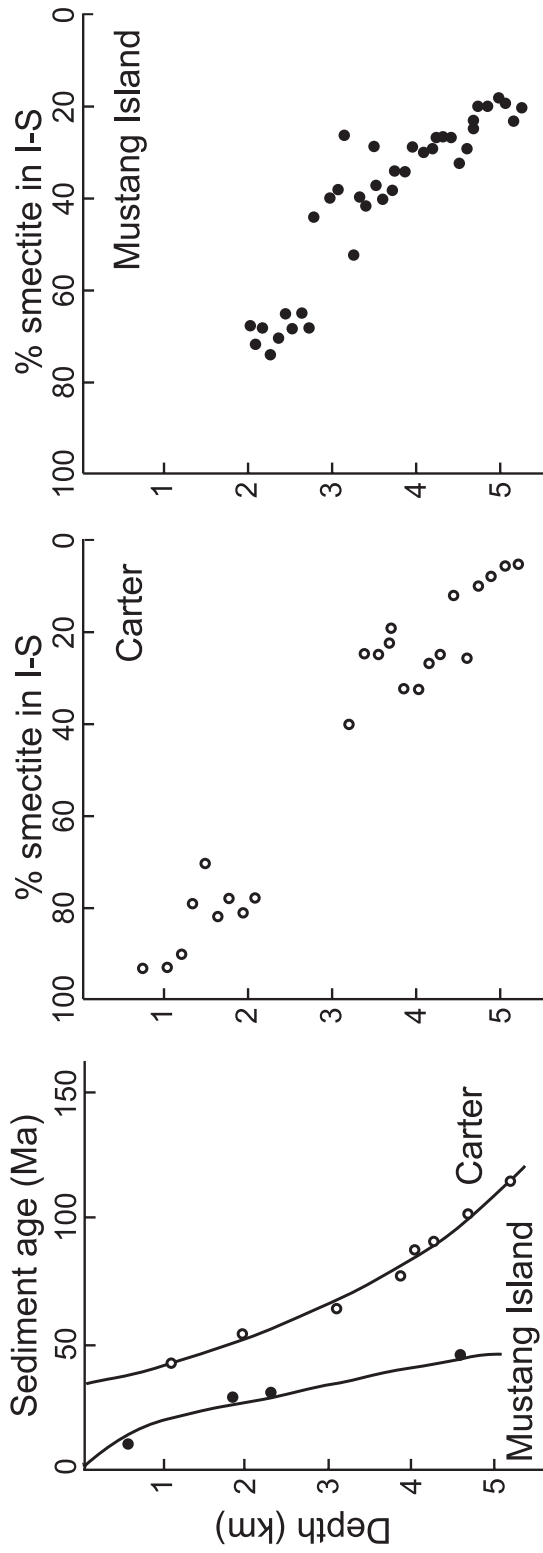
Fig. 1. Age of the sediments as a function of depth in Carter and Mustang Island wells (top—Velde and Vasseur, 1992). Smectite content in I-Exp as determined by Velde and Vasseur (1992) as a function of depth in these two wells.

Ca-saturated. Suspensions were kept in contact with a 1M $CaCl_2$ solution for 4 to 12 hours at room temperature to ensure a complete cation exchange. After three replications of this procedure, the excess chloride was rinsed with distilled water (Milli-Q—18.2 $M\Omega.cm^{-1}$).

Oriented preparations were obtained by pipetting a slurry of the Ca-saturated suspensions on a glass side and drying this suspension at 40°C for a few hours to obtain an air-dried (AD) preparation. Ethylene-glycol (EG) solvation of the slides was achieved by exposing them to EG vapor at 70°C for a minimum of 12 hours. XRD patterns were recorded with a Bruker D5000 powder diffractometer equipped with a Kevex Si(Li) solid state detector using $CuK\alpha_{1+2}$ radiation. Intensities were recorded at 0.04° 2θ step intervals from 2 to 50°, using a 6 sec counting time per step except for sample D (40 sec/step). Sizes of the divergence slit, the two Soller slits, the antiscatter, and resolution slits were 0.5°, 2.3°, 2.3°, 0.5° and 0.06°, respectively. Humidity was controlled at 40 percent RH for AD measurements.

XRD Profile Modeling

Structure models were determined using the multi-specimen method described by Drits and others (1997a), and Sakharov and others (1999a, 1999b). In contrast to usual identification methods of mixed layers, the multi-specimen method requires recording XRD patterns after different treatments for each sample. For a given sample, these patterns usually differ significantly because of the contrasting hydration/expansion behavior of expandable interlayers in response to these treatments. The method itself relies on the direct comparison of experimental profiles with those calculated for a structure model, the optimum agreement between data and calculated patterns being obtained by a trial-and-error procedure.

The different treatments affect the thickness and scattering power (nature, amount, and position of interlayer species) of the expandable interlayers, but not the layer sequences within the crystallites. As a consequence, a consistent structure model is obtained for a given mixed layer when layer sequences obtained from all experimental profiles of a given sample are nearly identical. XRD pattern modeling provides also a quantitative phase analysis of the samples. One essential requirement for structure model soundness is that the relative weight contributions of periodic and interstratified phases to the different XRD patterns of a given sample must be similar (Sakharov and others, 1999b; Claret, ms, 2001; Lindgreen and others, 2002; McCarty and others, 2004, 2005).

Structure models for each mixed layer include the number of the different layer types (not limited to 2), their nature and relative proportions. Markovian statistics are used to describe possible layer stacking sequences and the relative abundance thereof. An important parameter of this statistical description is the Reichweit parameter R (Jagodzinski, 1949) which characterizes the extent of ordering as the number of adjacent layers influencing the nature of a given layer. For R = 0, layer types are thus randomly interstratified, whereas for R = 1 the occurrence probability of a given layer type depends on the nature of its nearest predecessor. For a given value of the R parameter, a set of probability parameters is needed to completely describe layer stacking. The relative content of the different layer types (W_i) is systematically needed together with junction probability parameters (P_{ij}). P_{ij} parameters define the probability for a j-type layer to follow an i-type layer (i,j = I or Exp for I-Exp). W_i and P_{ij} parameters are related, and only two parameters are necessary to describe a two-component mixed layer with R = 1, W_I and P_{ExpExp} being commonly used for I-Exp. In this case, specific layer stacking modes for R = 1 include maximum possible degree of ordering (MPDO), which is obtained when pairs of the least abundant layers are prohibited in the stacking, that is when $P_{ExpExp} = 0$ assuming $W_I > W_{Exp}$. Random interstratification occurs when $P_{ExpExp} = P_{IExp} = W_{Exp} = 1 - W_I$, and physical mixture

of I and Exp layers when $P_{ExpExp} = 1$ whatever the W_{Exp} value. In addition, a tendency to segregation of i-type layers is characterized by $W_i < P_{ii}$ (i = I, Exp), whereas partial ordering occurs when $W_{Exp} > P_{ExpExp} > 0$ assuming $W_I > W_{Exp}$ (see Bethke and Altaner, 1986; Drits and Tchoubar, 1990; and Moore and Reynolds, 1997, for details).

The algorithm developed initially by Drits and Sakharov (1976) and used recently by Drits and others (1997a) and Sakharov and others (1999b) was used to fit experimental XRD profiles over the 2 to 50° 2θ range. Instrumental and experimental factors such as horizontal and vertical beam divergences, goniometer radius, length and thickness of the oriented slides were measured and introduced without further adjustment. Sigmastar (see Reynolds, 1986, for details) was set to 12 for all components of the clay paragenesis and the mass absorption coefficient (μ^*) to 45, as recommended by Moore and Reynolds (1997). In the profile fitting process, it was necessary to define different types of Exp layers as a function of their hydration or swelling behaviors in AD and EG states, respectively (Drits and others, 2002a). Irrespective of the hydration/swelling behavior of Exp layers, the relative contents of I and Exp layers and their stacking sequences should be the same in both AD and EG states. The hydration/swelling behavior of Exp layers is likely related to the amount and location of the layer-charge deficit, although this behavior may differ for a given layer from AD
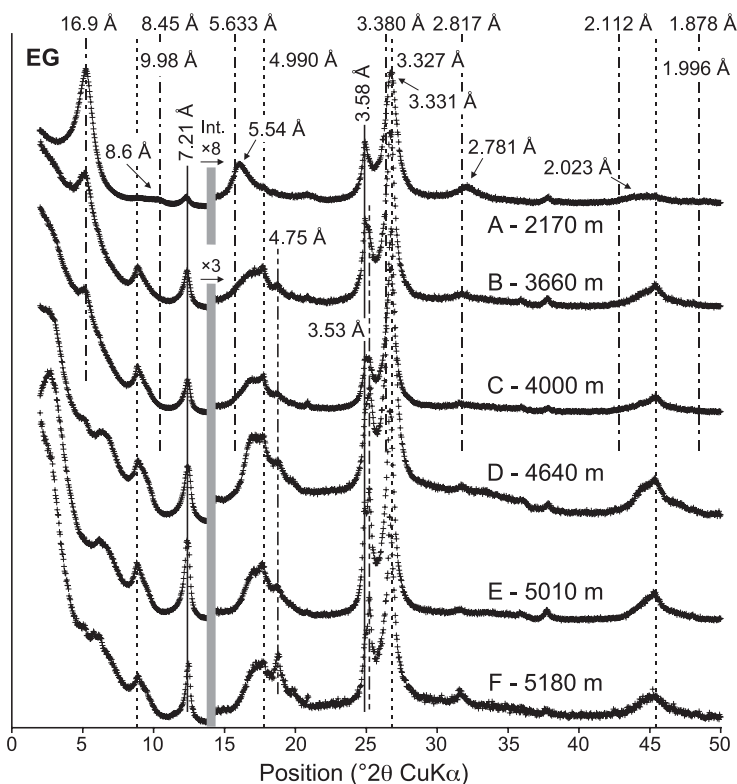
Fig. 2. Experimental XRD patterns obtained from Carter well samples selected as being representative of the complete smectite-to-illite diagenetic transition. Sampling depths are 2170 (A), 3660 (B), 4000 (C), 4640 (D), 5010 (E), and 5180 m (F). XRD patterns obtained on EG solvated samples. Dashed and dot-dashed lines indicate the positions of illite and smectite reflections. Solid and dot-dot-dashed lines indicate positions of some kaolinite and chlorite reflections. For all samples, the gray bar indicates a modified scale factor for the high-angle region.

to EG states. In the following I, K, Ch, and Exp denote illite, kaolinite, di-trioctahedral chlorite, and expandable layers, respectively. For all layer types z atomic coordinates proposed by Moore and Reynolds (1997) were used after modification to fit the layer thickness values used for simulation; thermal motion parameters (B) were also set as proposed by Moore and Reynolds (1997). The position and amount of interlayer species (H_2O and EG molecules in particular) were considered as variable parameters and varied about the values proposed by Moore and Reynolds (1997) during the fitting process. In bi-hydrated Exp layers (2W), a single plane of H_2O molecules was assumed to be present on each side of the interlayer mid-plane as proposed by Ferrage and others (2005a, 2005b).

Finally, distributions of coherent scattering domain sizes (CSDSs) were assumed to be lognormal and characterized by their mean value (Drits and others, 1997b). Quality of fit was assessed over the 4 to 50°2θ (22.0-1.85 Å) range with the R_{wp} and R_{exp} factors (Howard and Preston, 1989).

<div align="center">RESULTS</div>

Qualitative Description of the Experimental XRD Patterns

Evolution of sample structure with depth is best seen on XRD patterns obtained after EG solvation (fig. 2A). The XRD pattern of sample A (2170 m) exhibits a strong peak at ~16.9 Å, well resolved on its low-angle side, and weaker peaks at 8.6, 5.54, 3.331, 2.781, and 2.023 Å that form a non-rational series. In addition, peaks at 7.21, 3.58 and 2.38 Å and weak modulations at ~10.0 and 5.0 Å correspond to finely dispersed kaolinite and to discrete illite, respectively. The peak at ~17.0 Å is still
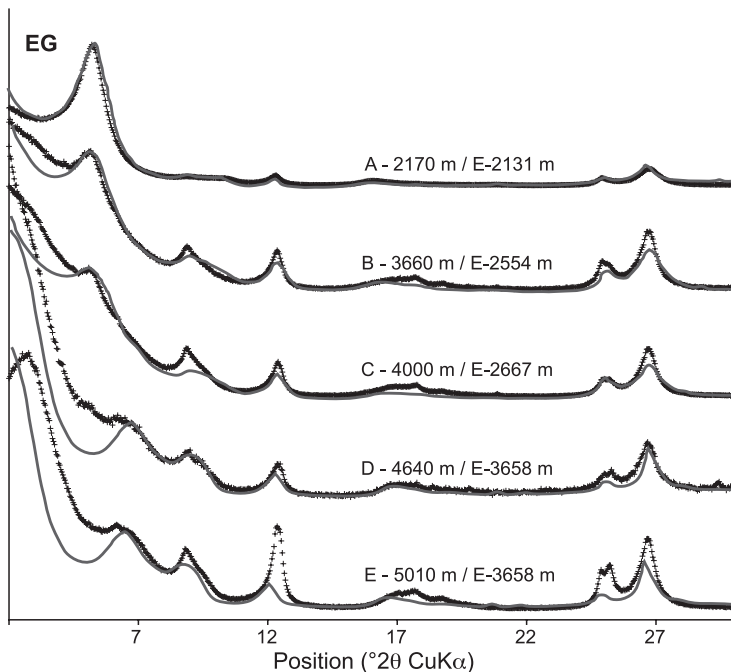
Fig. 3. Comparison between experimental XRD patterns obtained from Carter well samples investigated in the present study and those obtained by Perry and Hower (1970) on selected samples from well E (Galveston county). The latter samples were used to establish the smectite-to-illite diagenetic transition in Gulf Coast clay rich sediments. XRD patterns obtained on EG solvated samples.
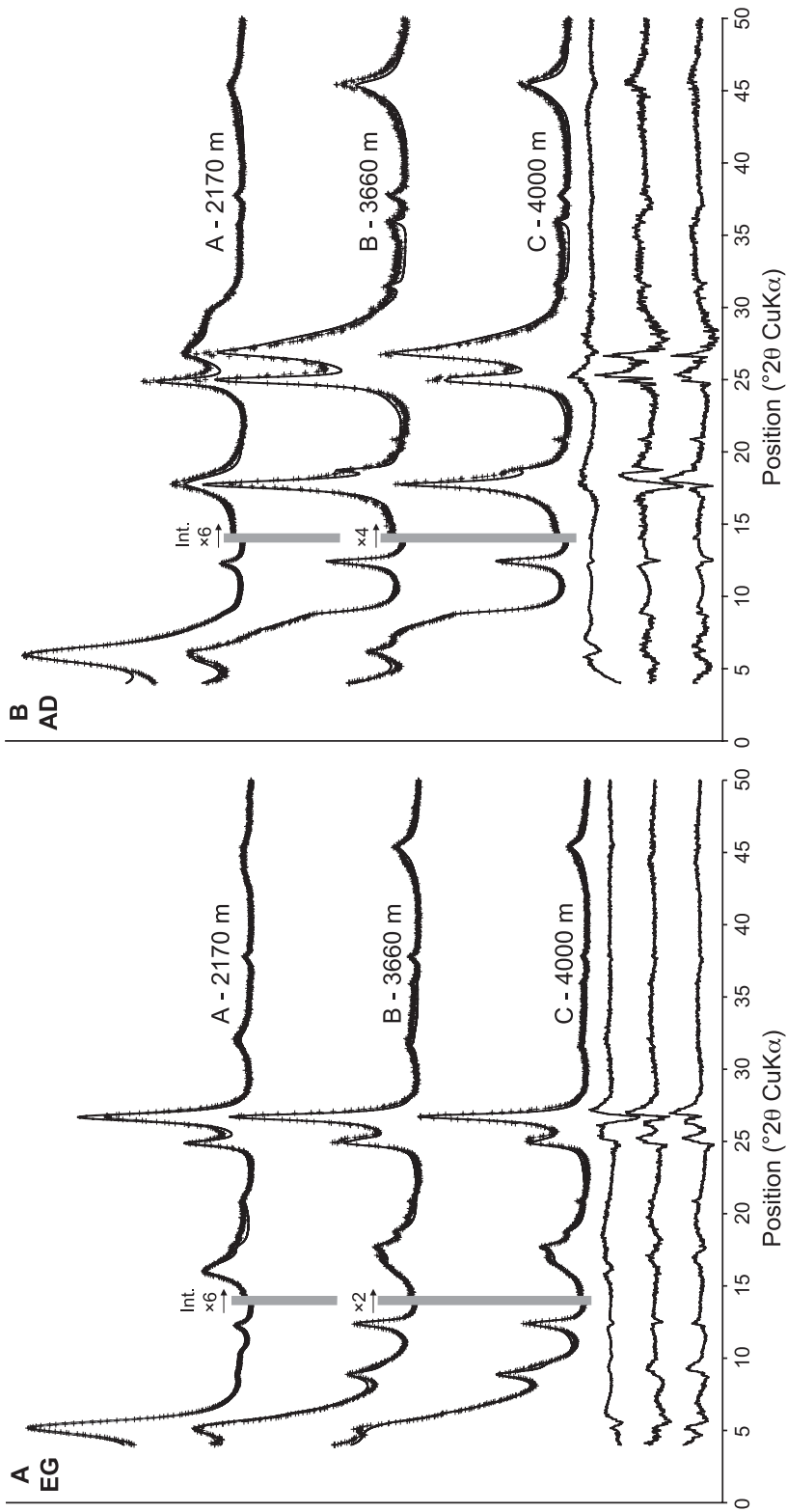
Fig. 4. Comparison between experimental and calculated XRD patterns as a function of depth for group I samples (single-phase segregated 1-Exp model). Experimental and calculated optimal XRD patterns are shown as crosses and as solid lines, respectively. Optimal structure models are described in tables 1 and 2. For all samples, the gray bar indicates a modified scale factor for the high-angle region. (A) XRD patterns obtained on EG solvated samples. (B) XRD patterns obtained on air-dried samples at 40% relative humidity.

*Single-phase segregated I-Exp model. Composition and structural parameters of the
segregated I-Exp in group I samples*

Sample	W_I	W_{Exp1}	W_{Exp2}	W_{Exp3}	h_{Exp1}	h_{Exp2}	h_{Exp3}	R	N_{av}	N_{max}	S_q
A – EG	0.45	0.55	-	-	16.76	-	-	1	7	50	
A – AD	0.45	0.30	0.15	0.10	15.00	12.50	14.00	1	7	50	0.27
B – EG	0.65	0.27	0.08	-	16.76	14.00	-	1	15	50	
B – AD	0.65	0.21	0.14	-	15.00	12.50	-	1	15	50	0.19
C – EG	0.65	0.27	0.08	-	16.76	14.00	-	1	15	50	
C – AD	0.65	0.15	0.20	-	14.90	12.50	-	1	15	50	0.10

Note: The basal d_{001} distances of the different layer types (h_i) are given in Å. R is the Reichweit
parameter (Jagodzinski, 1949) which characterizes the extent of ordering as the number of adjacent
layers influencing the nature of a given layer. N_{av} and N_{max} are the average and maximum numbers of
layers in coherent scattering domains (lognormal size distribution). S_q parameter is an estimator of the
degree of segregation in I-Exp (eq 1).

intense for sample B (3660 m) but its resolution is significantly reduced on its
low-angle side. Compared to sample A, the reflections at 5.54 Å and 2.781 Å are shifted
to higher and lower angles, respectively, in the XRD pattern of sample B. The
reflection at 8.6 Å (sample A) is shifted also to lower angles and appears as a high-angle
shoulder of the 10.0 Å reflection (sample B). XRD patterns of samples B and C are
alike, except that the low-angle resolution of the ~17.0 Å peak is reduced for sample C
compared to sample B. Samples B and C also contain significant amounts of discrete
illite and kaolinite, and a small amount of chlorite.

XRD patterns of samples taken from depths > 4500 m (D, E, and F) are all akin
and their profiles strongly differ from those of samples A, B and C. Over the low-angle
region, there is no peak at ~17.0 Å, but broad maxima between ~13.5 to 15.0 Å (fig.
2). These patterns also contain a super-reflection at ~30 Å, best seen for sample E, and
additional broad maxima at ~9.25 to 9.30 Å, and 5.20 to 5.25 Å. The low resolution of
the latter reflections results to some extent from their partial overlap with illite peaks at
10.0 Å and 5.0 Å. Finally, sharp kaolinite and chlorite reflections are visible at 3.579 Å
and 3.528 Å.

To summarize the above observations, the six samples can be divided in two
groups. XRD patterns of group I (samples A, B, and C) exhibit a ~17.0 Å reflection
(EG state) whose low-angle resolution decreases with increasing depth. XRD patterns
of group II (samples D, E, and F) exhibit a broad maximum at ~13.5 to 15.0 Å and a
super-reflection at ~30 Å. XRD patterns collected in AD conditions are shown in the
Appendix (fig. A-1).

The described evolution of XRD patterns with depth is typical for smectite
illitization resulting from the burial diagenesis of clay-rich rocks. For example, XRD
patterns presented by Perry and Hower (1970) for samples E-2131 m, E-2554 m, and
E-2667 m are almost superimposed (except for the kaolinite reflections) to those of
samples A, B and C, respectively (fig. 3). Similarly, the XRD pattern presented by Perry
and Hower (1970) for sample E-3658 m resembles that of samples D and E, except for
the low-angle intensity. According to Hower and others (1976) the observed evolution
is evidence for a continuous smectite-to-illite reaction series occurring through inter-
mediate mixed layers. However in both the Perry and Hower (1970) and Hower and
others (1976) studies, XRD pattern interpretation was restricted to a qualitative
comparison with patterns calculated for two-component I-Exp (EG) models. The
relative proportions of I and Exp layer types (W_i), and their ordering (P_{ij} parameters)
were the two essential parameters refined.

<p style="text-align:center">TABLE 1B</p>

<p style="text-align:center">*Single-phase segregated I-Exp model. Junction probabilities of the segregated IExp in samples A, B, and C*</p>

A-AD	I 9.98 Å	Exp1 15.00 Å	Exp2 12.50 Å	Exp3 14.00 Å
I (9.98 Å) 0.45	0.600	0.133	0.133	0.133
Exp1 (15.00 Å) 0.30	0.200	0.500	0.167	0.133
Exp2 (12.50 Å) 0.15	0.400	0.333	0.267	0.000
Exp3 (14.00 Å) 0.10	0.600	0.400	0.000	0.000

A-EG	I 9.98 Å	Exp 16.76 Å
I (9.98 Å) 0.45	0.600	0.400
Exp (16.76 Å) 0.55	0.327	0.673

B-AD	I 9.98 Å	Exp1 15.00 Å	Exp2 12.50 Å
I(9.98 Å) 0.65	0.716	0.178	0.106
Exp1 (15.00 Å) 0.21	0.520	0.350	0.130
Exp2 (12.50 Å) 0.14	0.537	0.150	0.313

B-EG	I 9.98 Å	Exp1 16.76 Å	Exp2 14.00 Å
I (9.98 Å) 0.65	0.716	0.216	0.068
Exp1 (16.76 Å) 0.27	0.520	0.480	0
Exp2 (14.00 Å) 0.08	0.550	0	0.450

C-AD	I 9.98 Å	Exp1 15.00 Å	Exp2 12.50 Å
I (9.98 Å) 0.65	0.684	0.138	0.178
Exp1 (14.90 Å) 0.15	0.600	0.150	0.250
Exp2 (12.50 Å) 0.20	0.580	0.240	0.180

C-EG	I 9.98 Å	Exp1 16.76 Å	Exp2 14.00 Å
I (9.98 Å) 0.65	0.683	0.249	0.068
Exp1 (16.76 Å) 0.27	0.600	0.400	0
Exp2 (14.00 Å) 0.08	0.550	0	0.450

TABLE 2

Single-phase segregated I-Exp model. Relative proportions (in wt%) of the different contributions to the diffracted intensity

Sample	I-Exp	Ill	Kaol	Ch	K-Exp[a]	R_{wp}[b]	R_{exp}[b]
A – EG	79	5	11	-	5	11.42%	1.73%
A – AD	79	5	11	-	5	11.00%	1.64%
B – EG	64	10	9	1	16	11.60%	2.36%
B – AD	57	13	9	2	19	10.80%	2.05%
C – EG	55	18	8	1	18	11.31%	1.94%
C – AD	52	25	8	2	13	9.85%	1.85%

[a] The composition of K-Exp is constant (75:25 K:Exp ratio).
[b] Estimators of the fit quality (R_{wp}) and of the statistical error associated with measured intensities (R_{exp}—Howard and Preston, 1989).

Quantitative Description of Experimental XRD Profiles

Group I samples: single-phase segregated I-Exp model.—According to this model, the non-rational series of basal reflections corresponds to a unique I-Exp in which I and Exp layers tend to segregate. XRD data are compared to calculated patterns in figure 4. Structural parameters used to calculate these patterns are listed in tables 1 and 2. Along with the main I-Exp contribution, samples contain kaolinite, illite (an illite-rich mixed layer with ~ 5% of expandable layers), minor chlorite, and a randomly interstratified K-Exp containing 75 percent kaolinite and 25 percent expandable layers. Although K-Exp have attracted considerably less attention than I-Exp, natural K-Exp covering the whole compositional range have been reported in the literature (see for example Sakharov and Drits, 1973; Sudo and Shimoda, 1977; Brindley and others, 1983). Consistent with these reports, K-Exp whose composition is dominated by kaolinite layers exhibit broad diffraction maxima shifted from the ideal kaolinite maxima towards the nearest smectite peaks as predicted by Méring (1949).

Transition from sample A to sample C corresponds to an increase in illite and K-Exp content (from 5 to ~21%, and from 5 to ~15%, respectively—table 2) and to a decrease of I-Exp (from 79 to ~53%). The kaolinite and chlorite content is about constant. With increasing depth, I-Exp expandability decreases from 55 percent in sample A to 35 percent in samples B and C (table 1A). Under AD conditions, three types of expandable layers (15.0, 12.5 and 14.0 Å layers) are found in I-Exp from sample A, whereas only 2W and 1W layers (15.0 and 12.5 Å, respectively) are encountered in samples B and C. After EG solvation all Exp layers in I-Exp from sample

TABLE 3

Single-phase segregated I-Exp model. Relative abundance of the different layers and layer pairs (W_i and W_{ij} parameters) for the segregated I-Exp in group I samples

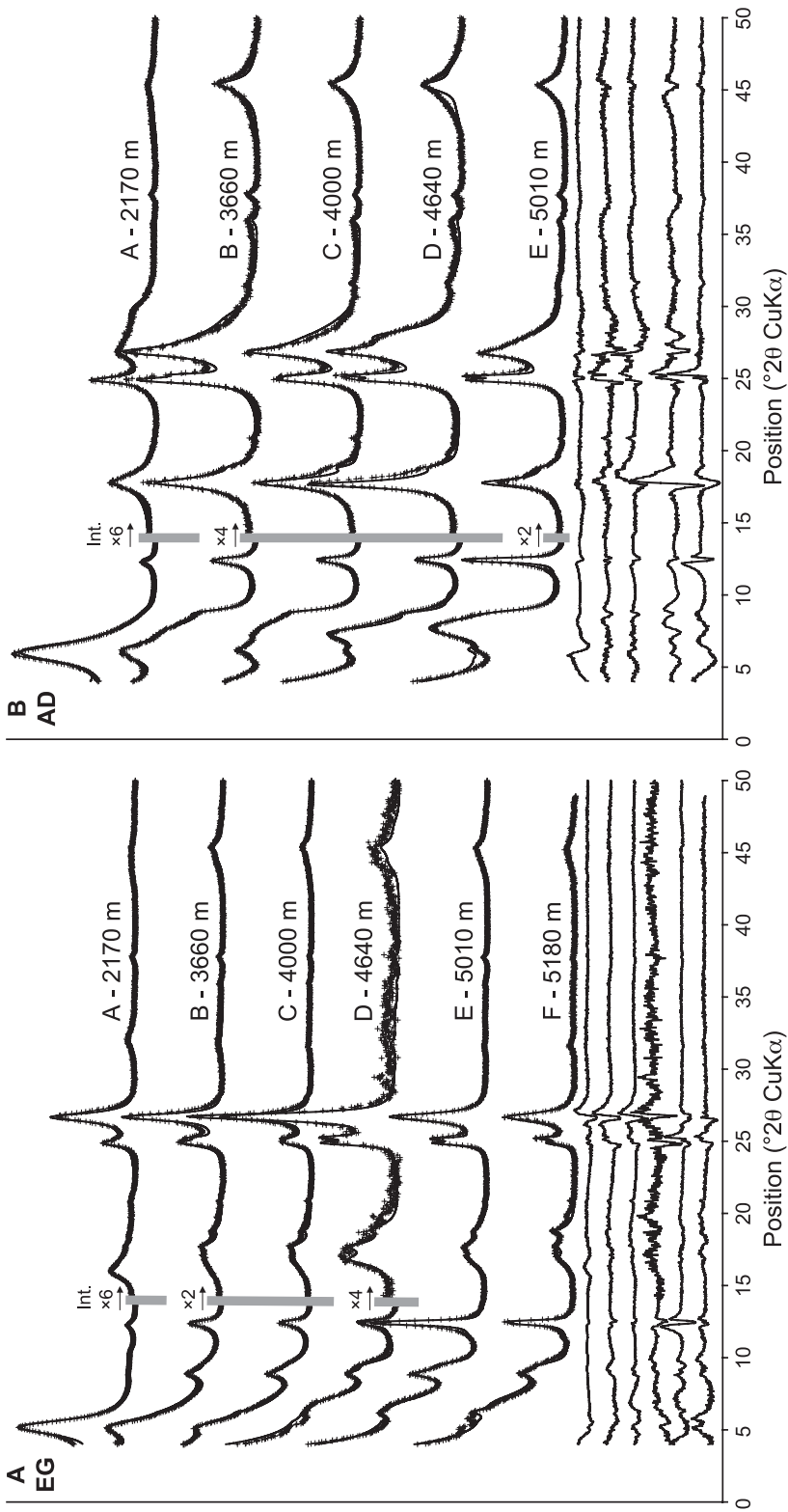| Layer sequence	A sample	B sample	C sample
I	0.45	0.65	0.65
Exp	0.55	0.35	0.35
II	0.270	0.465	0.444
IExp	0.180	0.184	0.206
ExpI	0.180	0.184	0.206
ExpExp	0.370	0.166	0.144

Fig. 5. Comparison between experimental and calculated XRD patterns as a function of depth for all Carter well samples (mixture model). Experimental and calculated optimal XRD patterns are shown as crosses and as solid lines, respectively. Optimal structure models are described in tables 4 and 5. For all samples, the gray bar indicates a modified scale factor for the high-angle region. (A) XRD patterns obtained on EG solvated samples. (B) XRD patterns obtained on air-dried samples at 40% relative humidity.

TABLE 4A

Mixture model. Composition and structural parameters of I-Exp in group I samples

Sample	Phase	W_I	W_{Exp1}	W_{Exp2}	W_{Exp3}	h_{Exp1}	h_{Exp2}	h_{Exp3}	N_{av}	N_{max}	R	Junction probability parameters $R = 0 \ (P_{ij} = W_j)$
A – EG	I-Exp	0.57	0.35	0.08	-	16.70	14.00	-	12	50	0	0
A – AD	I-Exp	0.57	0.20	0.08	0.15	15.00	14.00	12.50	12	50	0	0
B – EG	I-Exp	0.62	0.30	0.08	-	16.72	14.00	-	12	50	0	0
B – AD	I-Exp	0.62	0.15	0.08	0.15	15.00	14.00	12.50	12	50	0	0
C – EG	I-Exp	0.67	0.30	0.03	-	16.85	14.00	-	12	50	0	0
C – AD	I-Exp	0.67	0.17	0.03	0.13	15.00	14.00	12.50	12	50	0	0

Note: The basal d_{001} distances of the different layer types (h_i) are given in Å. R is the Reichweit parameter (Jagodzinski, 1949) which characterizes the extent of ordering as the number of adjacent layers influencing the nature of a given layer. N_{av} and N_{max} are the average and maximum numbers of layers in coherent scattering domains (lognormal size distribution).

TABLE 4B

Mixture model. Composition and structural parameters of K-Exp

Sample	Phase	W_I	W_{Exp1}	W_{Exp2}	H_K	h_{Exp1}	h_{Exp2}	N_{av}	N_{max}	R	Junction probability parameters $R = 0 \ (Pij = Wj)$
A – EG	K-Exp	0.75	0.10	0.15	7.156	16.90	12.90	12	50	0	0
A – AD	K-Exp	0.75	0.05	0.20	7.156	15.00	12.50	12	50	0	0
B – EG	K-Exp	0.75	0.00	0.25	7.156	16.90	12.90	12	50	0	0
B – AD	K-Exp	0.75	0.00	0.25	7.156	15.00	12.50	12	50	0	0
C – EG	K-Exp	0.75	0.10	0.15	7.156	16.90	12.90	12	50	0	0
C – AD	K-Exp	0.75	0.00	0.25	7.156	15.00	12.50	12	50	0	0
D – EG	K-Exp	0.75	0.15	0.10	7.156	16.90	12.90	12	50	0	0
D – AD	K-Exp	0.75	0.05	0.20	7.156	15.00	12.50	12	50	0	0
E – EG	K-Exp	0.75	0.15	0.10	7.156	16.90	12.90	12	50	0	0
E – AD	K-Exp	0.75	0.00	0.25	7.156	15.00	12.50	12	50	0	0
F – EG	K-Exp	0.75	0.10	0.15	7.156	16.90	12.90	12	50	0	0

Note: The basal d_{001} distances of the different layer types (h_i) are given in Å. R is the Reichweit parameter (Jagodzinski, 1949) which characterizes the extent of ordering as the number of adjacent layers influencing the nature of a given layer. N_{av} and N_{max} are the average and maximum numbers of layers in coherent scattering domains (lognormal size distribution).

TABLE 4C

Mixture model. Composition and structural parameters of the mixed layers in group II samples

Sample	Phase	W_1	W_{Exp1}	W_{Exp2}	W_{Ch}	h_{Exp1}	h_{Exp2}	h_{Ch}	N_{av}	N_{max}	R	Junction probability parameters
D – EG	I-Exp	0.70	0.25	0.05		16.86	12.90		15	100	1	R = 1 with MPDO[a] $P_{Exp1Exp1} = P_{Exp1Exp2} = 0$ $P_{Exp2Exp1} = P_{Exp2Exp2} = 0$
	I-Exp-Ch	0.70	0.15	-	0.15	16.86		14.00[b]	12	50	1	$P_{Exp1Exp1} = P_{Exp1Ch} = P_{ChExp1} = 0.150$ $P_{ChCh} = 0.265$
D – AD	I-Exp	0.70	0.30			15.00			15	100	1	R = 1 with MPDO[a] $P_{Exp1Exp1} = 0$
	I-Exp-Ch	0.70	0.05	0.10	0.15	15.00	12.50	14.00[b]	12	50	1	$P_{Exp1Exp1} = P_{Exp2Exp1} = P_{ChExp1} = 0.050$ $P_{Exp1Exp2} = P_{Exp2Exp2} = P_{ChExp2} = 0.100$ $P_{Exp1Ch} = P_{Exp2Ch} = 0.150 \; P_{ChCh} = 0.265$
E – EG	I-Exp	0.75	0.21	0.04		16.92	12.90		15	100	2	$P_{Exp1Exp1} = P_{Exp1Exp2} = P_{Exp2Exp1} = P_{Exp2Exp2} = 0$ $P_{Exp1IExp1} = 0.350$[b]
	I-Exp-Ch	0.70	0.15		0.15	16.86		14.00[b]	12	50	1	$P_{Exp1Exp1} = P_{Exp1Ch} = P_{ChExp1} = 0.150$ $P_{ChCh} = 0.265$
E – AD	I-Exp	0.75	0.21	0.04		15.00	12.50		15	100	2	$P_{Exp1Exp1} = P_{Exp1Exp2} = P_{Exp2Exp1} = P_{Exp2Exp2} = 0$ $P_{Exp1IExp1} = 0.350$[b]
	I-Exp-Ch	0.70		0.15	0.15		12.50	14.00[b]	12	50	1	$P_{Exp1Exp1} = P_{Exp1Ch} = P_{ChExp1} = 0.150$ $P_{ChCh} = 0.265$
F – EG	I-Exp	0.75	0.20	0.05		16.86	12.90		15	100	2	$P_{Exp1Exp1} = P_{Exp1Exp2} = P_{Exp2Exp1} = P_{Exp2Exp2} = 0$ $P_{Exp1IExp1} = 0.300$ $P_{Exp1IExp2} = 0.050$[c]
	I-Exp-Ch	0.70	0.10		0.20	16.86		14.00b	12	50	1	$P_{Exp1Exp1} = P_{Exp1Ch} = P_{ChExp1} = 0.150$ $P_{ChCh} = 0.265$

[a] Maximum possible degree of ordering which prohibits pairs of the minor layers: $P_{jj} = 0$ if $W_j < 0.5$. Refer to Reynolds (1980), Drits and Tchoubar (1990), and Moore and Reynolds (1997) for additional details.
[b] Other junction probability parameters needed to describe layer stacking are $P_{Exp1IExp2} = P_{Exp2IExp1} = P_{Exp2IExp2} = 0$.
[c] Other junction probability parameters needed to describe layer stacking are $P_{Exp2IExp1} = P_{Exp2IExp2} = 0$.

A swell to 16.76 Å with two planes of EG molecules in their interlayers (2EG layers). Swelling behavior is more heterogeneous in samples B and C (table 1A). In all three samples, $W_I < P_{II}$ (table 1B) for I-Exp and illite layers are thus slightly segregated, as estimated by the S_q parameter (Drits and Tchoubar, 1990):

$$S_q = (P_{ii} - W_i)/(1 - W_i) \qquad\qquad (1)$$

To determine S_q, it is convenient to use P_{II} and W_I values so as to disregard the actual distribution of Exp layers. With increasing depth, the S_q parameter decreases from 0.27 to 0.19 and to 0.10 (samples A, B and C, respectively), indicating that interstratification of I and Exp layers tends to become random with increasing burial depth and illite content (table 1A). The CSDS of I-Exp increases with burial depth from 7 (sample A) to 15 layers (samples B and C—table 1A). For a given sample, the P_{ij} parameters refined for the I-Exp are different for AD and EG states (table 1B). This apparent inconsistency arises from the contrasting expansion behavior of Exp layers in AD and EG states, and vanishes if the hydration/swelling behavior of Exp layers is carefully analyzed (see Appendix for details).

Single-phase segregated I-Exp model: Intrinsic inconsistency of the model.—If I-Exp in group I samples represent a series of diagenetically altered mixed layers, the occurrence probabilities of I and Exp layers, and those of the different layer pairs and triplets (W_i, $W_{ij} = W_i \times P_{ij}$ and $W_{ijk} = W_i \times P_{ij} \times P_{jk}$, respectively—table 3) should evolve logically in the context of illitization. For the sake of simplicity, all expandable layers will be considered together in the following discussion. From these occurrence probabilities, transition from sample A to sample B appears logical as the illite enrichment (from 45% to 65% at 2170 and 3660 m, respectively) is associated with the decrease of occurrence probability for layer pairs, and layer triplets (not shown), containing Exp layers (table 3). At the same time, the segregation degree in I-Exp decreases from 0.27 (sample A) to 0.19 (sample B) because ExpExp pairs disappear faster than II pairs form $[(W_{ExpExp})_B - (W_{ExpExp})_A = -0.205$, and $(W_{II})_B - (W_{II})_A = 0.194$—table 3].

In the general illitization scheme, the steady evolution of a segregated I-Exp towards random interstratification is *a priori* consistent with a solid-state transformation. The observed decrease of the Sq parameter between samples B (0.19) and C (0.10) follows the same logic although illite contents are similar in the two samples (table 3). However, when looking at the different W_{ij} probabilities, the I-Exp evolution between samples B and C cannot be interpreted reasonably in the illitization context. This evolution implies indeed the formation of IExp and ExpI pairs at the expense of both II and ExpExp pairs $[(W_{II})_B > (W_{II})_C$—table 3]. The single-phase segregated I-Exp model is thus inadequate to describe the structural evolution of group I samples, and should be rejected.

Group I samples: The mixture model.—According to this model, the ~17 Å peak of group I samples corresponds to discrete smectite coexisting with a randomly interstratified I-Exp with a high content of illite layers ($W_I > 50\%$—Claret, ms, 2001; Drits and others, 2002b; Claret and others, 2004; Lanson and others, 2005; McCarty, 2005; Aplin and others, 2006; McCarty and others, 2008). Data are compared in figure 5 to XRD patterns calculated for this model. Table 4A contains the structural and probability parameters for the I-Exp contribution, whereas relative proportions of the different contributions to the diffraction patterns are reported in table 5. In all group I samples, the major contribution is I-Exp whose relative proportion increases with increasing burial depth from 44 percent to 50 percent and to 57 percent (samples A, B and C, respectively). Simultaneously, the content of discrete smectite decreases dramatically

Mixture model. Relative proportions (in wt%) of the different contributions to the diffracted intensity

Sample	I-Exp	I-Exp-Ch	Sm	Ill	Kaol	Ch	K-Exp	R_{wp}[a]	R_{exp}[a]
A – EG	45	-	27	4	9	-	15	9.14%	1.73%
A – AD	43	-	26	6	11	-	14	8.06%	1.64%
B – EG	51	-	5	15	14	2	13	14.16%	2.36%
B – AD	50	-	5	19	12	2	12	9.30%	2.05%
C – EG	57	-	2	21	6	2	12	11.12%	1.94%
C – AD	58	-	3	22	7	2	8	9.72%	1.85%
D – EG	42	26	-	10	6	4	12	8.23%	2.28%
D – AD	39	28	-	9	5	4	15	8.99%	1.15%
E – EG	34	30	-	9	11	4	12	10.23%	2.11%
E – AD	31	32	-	6	12	5	14	11.94%	2.00%
F – EG	34	42	-	5	7	5	7	13.38%	3.07%

[a] Estimators of the fit quality (R_{wp}) and of the statistical error associated with measured intensities (R_{exp}—Howard and Preston, 1989).

from 27 percent to 5 percent and ~2 percent in samples A, B and C, respectively. As for the single-phase segregated I-Exp model the content of discrete illite increases significantly with depth from 5 percent to ~17 percent and to 21 percent in samples A, B and C. I-Exp is randomly interstratified despite its high illite content that ranges from 57 percent to 62 and to 67 percent (samples A, B and C, respectively). I-Exp has the same mean (12 layers) and maximum (50 layers) CSDS in all group I samples (table 4A). A randomly interstratified K-Exp with 75 percent kaolinite layers completes the clay paragenesis. K-Exp exhibits broad diffraction maxima at ~6.8 to 7.0 and 3.4 to 3.5 Å both in AD state and after EG solvation (figs. A-2A, B).

Group II samples.—Along with 4 to 5 percent of chlorite, 5 to 10 percent of illite (with 5% Exp layers), 6 to 12 percent of kaolinite, all group II samples contain I-Exp, I-Exp-Ch and K-Exp mixed layers. The structural and probability parameters providing the best fit to XRD data (fig. 5) are reported in table 4C. The major phases are I-Exp and I-Exp-Ch. The relative proportion of I-Exp decreases slightly with burial depth from 40 percent (sample D) to 33 and 34 percent (samples E and F, respectively) whereas that of I-Exp-Ch steadily increases from 27 percent to 31 percent and to 42 percent (samples D, E and F, respectively).

Parallel to this phase composition change, transition from sample D to sample F is characterized by a slight increase of the illite content in I-Exp (from 70 to 75%). In sample D, interstratification of I and Exp layers is ordered (R = 1) with MPDO ($P_{Exp1Exp1} = P_{Exp1Exp2} = P_{Exp2Exp1} = P_{Exp2Exp2} = 0$). Longer-range ordering (R = 2—table 4C) is observed for samples E and F. In the latter samples P_{ij} parameters are similar to sample D, and longer-range ordering is characterized by a slight segregation of IExpIExp sequences as $P_{ExpIExp} > W_{Exp}/W_I$ (see Drits and Tchoubar, 1990, for details). Compared to I-Exp in group I samples, the size of I-Exp CSDs is significantly increased for group II samples (mean and maximum values are 15 and 100 layers compared to 12 and 50, respectively, for group I samples—tables 4A, C). In all group II samples, I-Exp-Ch contains 70 percent of illite layers interstratified with Exp and di-trioctahedral chlorite layers, the proportion of Ch layers increasing from 15 percent in samples D and E, to 20 percent in sample F. In contrast to the ordered I-Exp, I-Exp-Ch CSDs are similar to those determined for the I-Exp in group I samples (tables 4A, C). Finally, K-Exp (R = 0) consists of 75 percent kaolinite and 25 percent Exp layers as in group I samples.

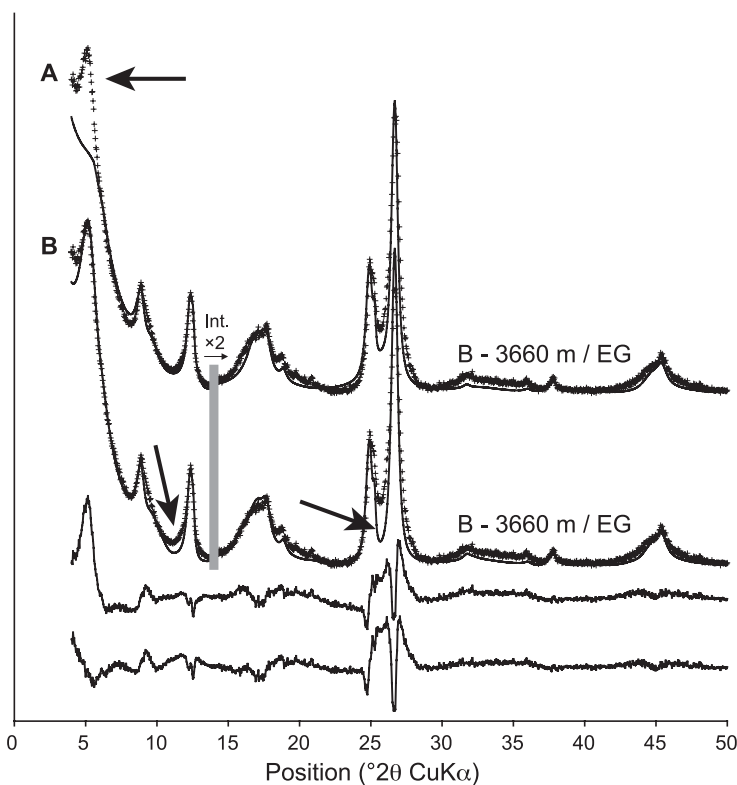492 *B. Lanson and others—Diagenetic smectite-to-illite transition in clay-rich*

Fig. 6. Sensitivity of calculated XRD patterns to the mineralogical composition. Patterns as for figure 5. Arrows indicate significant misfit as compared to the optimum fits shown in figure 5. The optimum mineralogical composition is given in table 5. (A) Sample B—3660 m Ca-saturated after EG solvation without the contribution of discrete smectite. (B) Sample B—3660 m Ca-saturated after EG solvation without the contribution of K-Exp.

<center>DISCUSSION</center>

Reliability of Structure Models

The results obtained in the present work demonstrate the ability of the multi-specimen approach to provide good quality fit to experimental data obtained on natural polyphasic samples, in agreement with previous studies (Drits and others, 1997a, 2002a, 2002b, 2004; Sakharov and others, 1999a, 1999b; Lindgreen and others, 2000, 2002; Claret and others, 2004; McCarty and others, 2004, 2008). This approach can thus be used to determine accurate structural parameters for the phases present in a given sample. In the present work, satisfactory fit to experimental positions, intensities and profiles of basal XRD reflections was obtained using up to three mixed layers, each incorporating from two to four layer types, in addition to discrete phases.

Obviously, the more discrete and mixed-layer phases that coexist in a sample, the more independent structural parameters that are needed for simulation. As a result, the reliability and accuracy in determining these parameters may decrease as more phases are introduced, although constraints are provided by the required uniqueness of structure models used to fit different patterns of a given sample (AD and EG patterns of Ca-saturated samples in the present case).

Evidence for the actual phase composition.—As the optimum fits to XRD data were obtained using a trial-and-error approach, the actual sensitivity of XRD simulations to
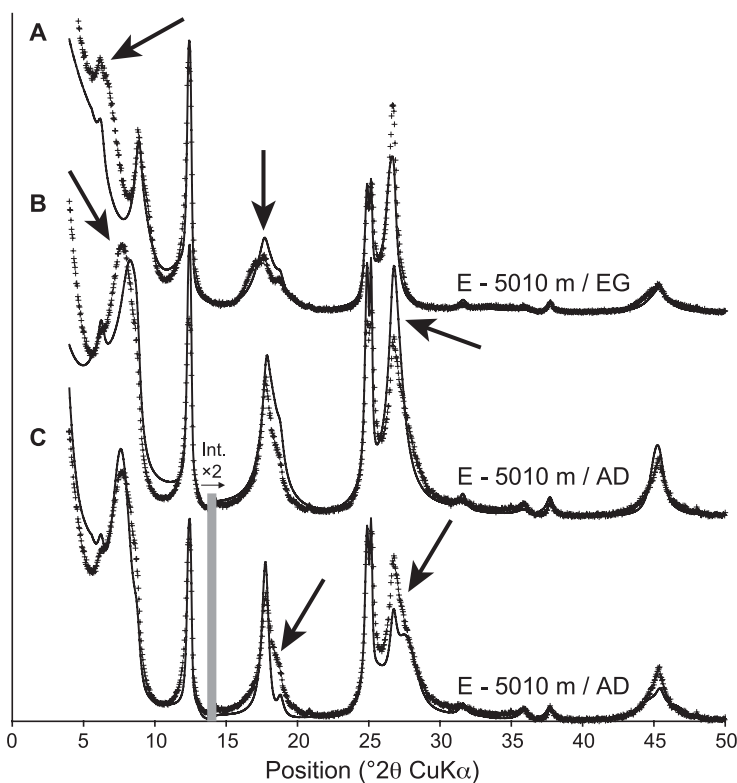
Fig. 7. Sensitivity of calculated XRD patterns to the mineralogical composition. Patterns as for figure 5. Arrows indicate significant misfit as compared to the optimum fits shown in figure 5. The optimum mineralogical composition is given in table 5. (A) Sample E—5010 m Ca-saturated after EG solvation without the contribution of I-Exp. (B) Sample E—5010 m Ca-saturated air-dried without the contribution of I-Exp. (C) Sample E—5010 m Ca-saturated air-dried without the contribution of I-Exp-Ch.

key structural parameters needs to be assessed. The presence of the different contributions is the first of these parameters, and samples B and E will be used as typical for group I and II, respectively. Elementary contributions to the intensity diffracted by these two samples are shown in the Appendix (figs. A-2, A-3). Figure 6 compares the XRD pattern of sample B with those calculated for models similar to the optimal one (fig. 5) after subtraction of the contributions of discrete smectite or of K-Exp. Logically, the absence of the minor smectite contribution leads to the absence of the 17 Å peak in the calculated EG pattern (fig. 6A—R_{wp} = 17.56%). Similarly, the absence of the K-Exp contribution leads to significant misfits at $\sim$11.5° and $\sim$26° 2θ (fig. 6B—R_{wp} = 16.00%).

For group II samples, exclusion of either I-Exp or I-Exp-Ch contributions in the calculated XRD pattern decreases dramatically the agreement with the data. For example, calculated intensity is reduced in the low-angle region if the I-Exp contribution is subtracted from the optimal fit (fig. 7A). Additional significant misfits are observed at 16 to 19° 2θ and 26 to 36° 2θ in both EG and AD XRD patterns (fig. 7A—R_{wp} = 23.04%, and fig. 7B—R_{wp} = 27.73%, respectively). Figure 7C (R_{wp} = 20.62%) shows that the I-Exp-Ch contribution is essential to fit the AD pattern in the 18 to 20 and 26 to 31° 2θ ranges. In the present work, mixed layers are introduced only if they allowed fitting specific angular ranges without significant overlap with other phases.
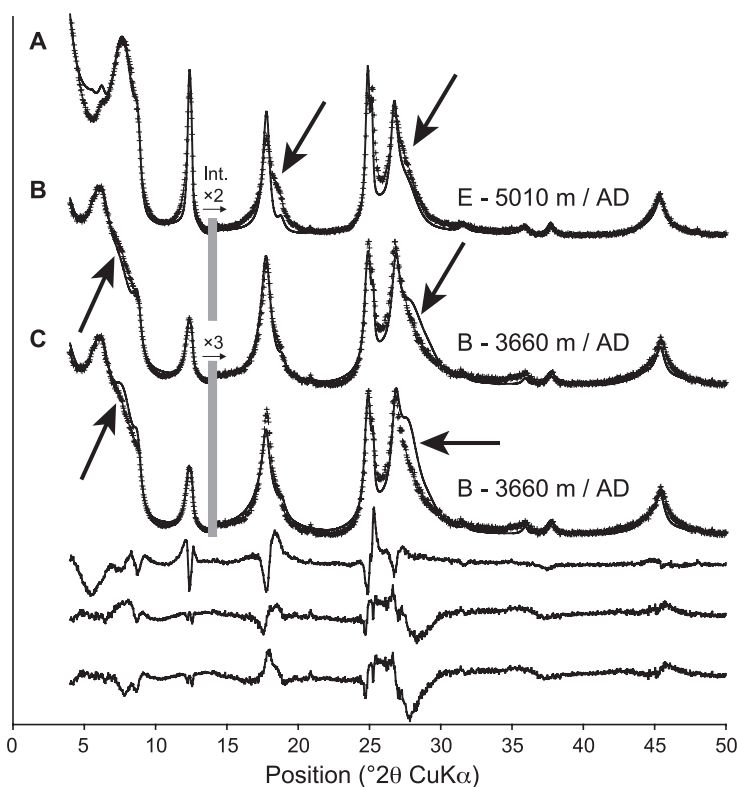
Fig. 8. Sensitivity of calculated XRD patterns to structural parameters. Patterns as for figure 5. Arrows indicate significant misfit as compared to the optimum fits shown in figure 5. The structural parameters for the optimal models are given in table 4. (A) Sample E—5010 m Ca-saturated air-dried. In I-Exp-Ch, Ch layers (with 3.0 Mg and 6.0 OH per half unit-cell in their interlayers) are replaced by Exp layers (with 0.25 Mg and 2.0 OH per half unit-cell in their interlayers). (B) Sample B—3660 m Ca-saturated air-dried. In I-Exp, 14.0 Å Exp layers (8% of the layers) are replaced by 15.0 Å Exp layers. (C) Sample B—3660 m Ca-saturated air-dried. In I-Exp, 14.0 Å Exp layers (8% of the layers) are replaced by 12.5 Å Exp layers.

Evidence for the presence of chlorite layers in I-Exp-Ch.—The actual nature of the mixed layer coexisting with the ordered I-Exp was determined after testing numerous illite-containing structure models with contrasting amounts, and distributions, of Exp layers: in addition to I and Exp layers the optimum mixed layer (I-Exp-Ch) contains di-trioctahedral layers consisting of dioctahedral 2:1 layers and of trioctahedral brucite-like interlayer sheets. Despite a similar basal spacing, the 14.0 Å Ch layers can be differentiated from 14.0 Å Exp layers because of their contrasting scattering factors. If Ch layers (with 3.0 Mg and 6.0 OH per half unit-cell in their interlayers) are replaced by Exp layers (with 0.25 Mg and 2.0 H_2O per half unit-cell in their interlayers), significant misfits are visible at 17 to 18° and 26 to 31° 2θ for sample E (fig. 8A—R_{wp} = 17.41%). XRD patterns calculated for the optimum I-Exp-Ch contribution and for the contribution in which Ch layers are replaced by Exp layers are shown in figure A-4. The strong intensity increase at 17 to 18° 2θ induced by the presence of Ch layers is related to the specific intensity distribution observed for sudoite (di-trioctahedral chlorite), whose 4.7 Å reflection is most intense (Lin and Bailey, 1985; Billault and others, 2002; Kameda and others, 2007).

Heterogeneous hydration/swelling of Exp layers.—In both AD and EG states, Exp layers present in mixed layers often exhibit various interlayer configurations and *d*-spacings

as reported for reference smectite samples (Ferrage and others, 2005b, 2007). For example, in the AD state I-Exp from group I samples systematically contains 15.0, 14.0 and 12.5 Å layers (table 4). Sensitivity of XRD to such heterogeneous behavior may be assessed by replacing, for example, 14.0 Å Exp layers (8% of the layers in I-Exp from sample B) either by 15.0 Å or by 12.5 Å layers (figs. 8B and C, respectively). In both cases, significant misfits are visible at 28 to 30° 2θ.

Diagenetic Illitization of Clay-rich Sediments: A Two-Stage Process

Undoubtedly, illitization of clay-rich sediments during burial diagenesis of mudstones and shales ranks among the most important and most documented mineral reactions. In the present work, the innovative interpretation of XRD patterns provides detailed information on the different phases present in the sediments and on their evolution. As a result, a structural mechanism can be proposed which contrasts with the usual description of a continuous transformation described by Perry and Hower (1970), Hower and others (1976) and many other authors (see Srodon, 1999, for a review). According to this commonly accepted model, diagenetic illitization of clay-rich sediments consists of two main stages whose existence is not challenged in the present study. The evolution of the mineralogical composition, and the structural evolution of individual phases will thus be described separately for group I and group II samples.

Smectite illitization in the upper part of the series (group I samples).—The commonly accepted model assumes the steady illitization of a unique randomly interstratified I-Exp. By contrast two phases, a discrete smectite and a randomly interstratified I-Exp with high illite content, coexist in group I samples in addition to discrete illite, kaolinite, K-Exp and chlorite (except for sample A). When burial depth increases the relative proportion of discrete smectite decreases sharply from 27 percent at 2170 m to 2 to 3 percent at 4000 m and the illite content in I-Exp increases (from 57% to 67% at the same depths). Except for a few early reports (Perry and Hower, 1970, 1972; Reynolds and Hower, 1970; Bethke and others, 1986), randomly interstratified I-Exp with such high illite contents have seldom been described in diagenetic environments, interstratification of I and Exp layers being usually described as ordered (R = 1 and MPDO) when illite layers prevail. However, the coexistence of discrete smectite with randomly interstratified I-Exp with high illite content is possibly widespread at shallow depth in sedimentary basins, the absence of significant maximum in the low-angle region being responsible for their scarce description. The steady decrease of the 17.0 Å peak intensity and of its low-angle resolution observed with depth for group I samples is indeed characteristic of the early stage of the diagenetic smectite-to-illite transition (fig. 3).

A similar mineralogical composition was described in the Callovo-Oxfordian sedimentary formation (Paris Basin—Claret, ms, 2001; Claret and others, 2004). Using the same methodological approach McCarty (2005), and McCarty and others (2008) also demonstrated that discrete smectite and randomly interstratified I-Exp with high illite content coexist in shallow samples from the off-shore Gulf Coast. The similarities between the XRD patterns recorded for group I samples and those obtained from Gulf Coast wells B and E by Perry and Hower (1970, 1972) support such a coexistence in the latter samples. TEM observations performed on shallow samples from various sedimentary basins also support the ubiquity of such a clay paragenesis (Freed and Peacor, 1992; Dong and others, 1997; Dong, 2005).

I-Exp in group I samples are characterized also by heterogeneous hydration/swelling behavior of Exp layers. In the AD state, 1W ($d_{001} \sim 12.5$ Å) and 2W ($d_{001} \sim$ 15.0 Å) layers systematically coexist in I-Exp (table 4), most likely as a consequence of the heterogeneous distribution of the amount and/or location of the layer-charge deficit. However, layer-charge heterogeneity is likely not considerable as both layer

types swell to 16.7 to 16.9 Å following EG solvation (table 4). In addition, I-Exp includes 14.0 Å layers present in similar proportions under AD and EG conditions. These layers cannot be considered as smectite layers as their basal spacing remains constant upon EG solvation, and their actual nature is unclear. Their basal spacing and swelling behavior are consistent with hydroxy-interlayered vermiculite layers that are often found in soils as a separate phase (Douglas, 1989; Moore and Reynolds, 1997; Chen and others, 2001; Marques and others, 2002). The observed hydration/swelling heterogeneity of Exp layers is most likely common in natural samples, thus impairing the potential of most usual identification methods for I-Exp as discussed in more detail by McCarty and others (2008).

Group I samples: origin of the randomly interstratified I-Exp with high illite content (~65%I).—It is commonly assumed that the smectite-to-illite reaction starts from a pure smectite precursor. However, Hower and others (1976) pointed out that in young sedimentary basins the pure smectite stage may be concealed by the high variability of smectite contents in randomly interstratified I-Exp from surface samples. According to Jennings and Thompson (1986) and Velde and Vasseur (1992), the compositional homogenization of I-Exp, likely through its recrystallization and formation of pure smectite, occurs at burial depths ranging typically from several hundred meters in older rocks to 1 to 2 km in younger ones. Smectite then acts as a precursor for the diagenetic smectite-to-illite conversion (Velde and Iijima, 1988). In the Carter well, the presence of pure smectite was inferred at 683 m from XRD analysis (Berger and others, 1999). In the present study, no XRD data were collected over the 683 to 2150 m depth interval. It is however reasonable to assume that steady smectite-to-illite conversion occurs over this depth interval, and that both smectite and I-Exp are authigenic in group I samples. Additional support for the authigenic origin of I-Exp comes from the similar XRD patterns obtained in this study and from other Gulf Coast samples (Perry and Hower, 1970, 1972). The diagenetic smectite-to-illite sequences described by the latter authors start from very smectitic material and subsequently evolve to form parageneses having XRD patterns very similar to those of group I samples (fig. 3).

Group I samples: new description of smectite illitization during the first stage.—From the present interpretation of XRD patterns, the shallow part of the diagenetic smectite-to-illite sequence thus corresponds to the formation of a randomly interstratified I-Exp with prevailing illite layers ($W_I > 50\%$) at the expense of smectite which is present as a pure phase in the shallowest samples. At burial depths lower than 4000 m, the overall smectite-to-illite conversion thus results i) from the dissolution of pure smectite, and ii) from the formation of the randomly interstratified I-Exp with $W_I > W_{Exp}$. The latter process is likely fed by smectite dissolution and favored by K-availability. The overall (I-Exp + smectite) content decreases with increasing burial depth (from ~70% in sample A to ~60% in sample C) possibly because smectite dissolution does not only feed I-Exp formation. Several important conclusions derive from these results.

The first stage of smectite illitization is heterogeneous, with the simultaneous progress of smectite dissolution and of I-Exp illitization, in agreement with electron microscopy observation of Gulf Coast shales (Freed and Peacor, 1992; Dong and others, 1997; Dong, 2005). As a consequence, pure smectite is present at significant burial depth, indicating a much higher stability than commonly accepted. In the Carter well for example, pure smectite which accounts for most of the clay fraction at 683 m (Berger and others, 1999) persists down to ~4000 m depth where it still represents 2 percent of the clay fraction (table 5). Although in the investigated samples smectite illitization proceeds simultaneously with partial smectite dissolution, the two reactions do not appear to be systematically linked. For example, Claret and others (2004) present evidence that I-Exp composition is constant while smectite is steadily

dissolving over a narrow depth interval in the Callovo-Oxfordian formation (eastern Paris basin). Similarly, McCarty (2005) and McCarty and others (2008) describe important variations of discrete smectite relative proportion without any compositional evolution of the coexisting I-Exp.

The new description also raises the need to reconsider the kinetics of smectite illitization. According to the usual identification criteria (for example Srodon, 1981; Inoue and others, 1989), XRD data obtained from the Carter samples correspond to an I-Exp with ~ 20 percent illite layers (R = 0) down to ~2000 m depth (Velde and Vasseur, 1992; Berger and others, 1999). Similarly, shallow samples from Gulf Coast wells are dominated by randomly interstratified I-Exp with ~25 percent illite layers according to Perry and Hower (sample E −1829 m—1970, 1972). By contrast, XRD profile modeling shows that I-Exp contains 57 percent illite layers at similar depth (sample A). Illitization is thus faster than commonly assumed as randomly interstratified I-Exp with $W_I > W_{Exp}$ likely forms under shallow burial conditions consistent with the TEM observations of Freed and Peacor (1992). The formation of a randomly interstratified I-Exp having a given composition thus occurs at much lower temperature than assumed from the commonly accepted model of smectite illitization for similar conditions of burial diagenesis (pressure, K activity, water-rock ratio, *et cetera*). The illite content in I-Exp obtained from both approaches may however be partially reconciled by taking into account the contribution of pure smectite. When this contribution is minimum (2%—sample C), similar compositions are determined for I-Exp (~65%I) using either the usual identification criteria (3500-4000 m deep samples in Carter well, fig. 1—Velde and Vasseur, 1992; Berger and others, 1999) or the present modeling approach.

In any case, the rate of smectite illitization strongly decreases with increasing burial depth, in contrast with the commonly accepted model (see for example Srodon and Eberl, 1984). According to the present data, the illite content in I-Exp increases at a minimum rate of 40%I/km from 683 to 2170 m depth. By contrast, from 2170 m to 4000 m the increase of illite content in I-Exp is limited to ~10 percent (table 4), at a rate of ~5%I/km. In agreement with Berger and others (1999), this rate decrease is likely due to the low amount of available K, in relation with the dissolution of K-feldspars and micas. In the studied samples, the maximum illitization rate coincides with the dissolution of K-feldspars which disappear at ~2000 m in the Carter well (Berger and others, 1999).

Structural evolution of clay minerals during deep burial diagenesis (group II samples). —The presence of a unique illite-rich ordered (R ≥ 1) I-Exp is characteristic of deep burial diagenesis in the commonly accepted model for smectite illitization. According to the present modeling results, such a phase is actually present in group II samples coexisting with another illite-containing mixed layer. In addition to illite and Exp layers, the latter structure includes di-trioctahedral chlorite layers, whose formation is consistent with the low K-availability (Whitney and Northrop, 1988) and whose relative proportion increases slightly with increasing burial depth (table 4). Interstratification of the different layer types is almost random in I-Exp-Ch, with only a slight tendency to segregation of Ch layers. By contrast, the slight increase of the illite content in I-Exp is associated with a steady increase of layer ordering. Specifically, the succession of dominant illite layers is favored and the extent of this ordering (quantified by the Reichweit R parameter—Jagodzinski, 1949; Reynolds, 1980) tends to increase beyond the nearest neighbor with increasing burial depth (table 4).

Transition from group I to group II samples: structural evolution of I-Exp from group I to group II samples.—The illite content in I-Exp increases only slightly from sample C to sample D, whereas the layer distribution is dramatically modified between the two samples, interstratification being random in sample C and ordered (R =1 with MPDO)

Mixture model. Relative abundance of the different layers and layer pairs (W_i and W_{ij} parameters) in the I-Exp of samples C and D

Layer sequence	C sample	D sample
I	0.670	0.700
Exp1	0.300	0.250
Exp2	0.030	0.050
II	0.449	0.400
IExp1	0.201	0.250
IExp2	0.020	0.050
Exp1I	0.201	0.250
Exp1Exp1	0.090	0.000
Exp1Exp2	0.009	0.000
Exp2I	0.020	0.050
Exp2Exp1	0.009	0.000
Exp2Exp2	0.001	0.000

in sample D. In the context of smectite illitization, II pairs should be preserved and solid-state transformation can be hypothesized only if the relative proportion of IExp and ExpI pairs increases at the expense of the sole ExpExp pairs. On the contrary, it is clear from table 6 that ExpExp pairs originally present in sample C are not abundant enough (0.109) to account for the increase of IExp and ExpI pairs from sample C to sample D $[(W_{IExp} + W_{ExpI})_D - (W_{IExp} + W_{ExpI})_C = 0.158]$. The transition from sample C to sample D can thus only result from a dissolution-recrystallization process. Indirect support for the proposed mechanism comes from the extremely low intensity scattered by sample D, which required a seven-fold increase of the collection time to obtain a similar signal-to-noise ratio for a given amount of material. The low amplitude of the XRD signal is likely due to the presence of XRD-amorphous material whose presence is expected for a major dissolution-reprecipitation process. Additional indirect support arises from the significant CSDS increase observed for the I-Exp from sample C to sample D (table 5). No K-Ar ages are available for the samples investigated in the present study. However, Aronson and Hower (1976) reported significantly younger ages for deep Gulf Coast samples (typical of group II samples) than for shallower samples (typical of group I samples). The gap between the two groups of samples also supports a major dissolution-recrystallization process leading to the crystallization of an ordered I-Exp at the expense of a randomly interstratified I-Exp of similar composition.

Transition from group I to group II samples: possible solid-state formation of I-Exp-Ch at the expense of I-Exp.—The illite contents in I-Exp from sample C and in I-Exp-Ch from sample D are similar (67 and 70%I, respectively). Their junction probability parameters exhibit also strong similarities, interstratification being random in I-Exp from sample C, and showing only slight tendency to segregation in I-Exp-Ch from sample D (table 4C). In addition, I-Exp from sample C and I-Exp-Ch from sample D have similar CSDSs. It is thus possible to hypothesize a solid-state mechanism, involving Mg polymerization in former Exp interlayers, for the transition between the two mixed layers. In this case, a series of mixed layers with compositions intermediate between those of the two end members can be envisaged. In I-Exp from sample C and in

TABLE 7

Mixture model. Junction probabilities of mixed layers occurring during the hypothesized solid-state transformation of I-Exp from sample C to I-Exp-Ch from sample D. The composition and structural parameters (segregation of I and Exp layers) of these mixed layers are thus theoretically intermediate between those of the two end members

Layer sequence	Sample C	Inter. Phase I	Inter. phase II	Sample D
W_I	0.670	0.680	0.690	0.700
W_{Exp}	0.330	0.270	0.210	0.150
W_{Ch}	0.000	0.050	0.100	0.150
Sq - I	0.000	0.027	0.054	0.083
Sq - Ch	0.000	0.045	0.090	0.135
P_{II}	0.670	0.689	0.707	0.725
P_{IExp}	0.330	0.264	0.205	0.150
P_{ICh}	0.000	0.047	0.088	0.125
P_{ExpI}	0.670	0.680	0.690	0.700
P_{ExpExp}	0.330	0.270	0.210	0.150
P_{ExpCh}	0.000	0.050	0.100	0.150
P_{ChI}	-	0.561	0.573	0.585
P_{ChExp}	-	0.346	0.246	0.150
P_{ChCh}	-	0.093	0.181	0.265

Note: S_q is an estimator of the degree of segregation of I and Ch layers in I-Exp-Ch (eq 1).

I-Exp-Ch from sample D, Exp layers are randomly distributed within crystallites ($P_{Expi} = W_i$), whereas I and Ch layers are slightly segregated in sample D ($W_I < P_{II}$, and $W_{Ch} < P_{ChCh}$). The degree of segregation of I and Ch layers in I-Exp-Ch from sample D is 0.083 and 0.135, respectively (Eq. 1—table 4C). To propose compositional and structural parameters for intermediate phases, one may thus hypothesize that the increase of I and Ch contents from sample C to sample D is accompanied by the increase of their tendency to segregation. Probability parameters describing such theoretical intermediate phases (phases I and II) are reported in table 7. In particular, the relative proportions of I and Ch layers in these phases are equal to 68 percent and 5 percent (phase I) and 69 percent and 10 percent (phase II), respectively, to account for the compositional change from sample C (67%I and 0%Ch) to sample D (70%I and 15%Ch). In addition, the degrees of segregation of I and Ch layers increase steadily from sample C (0.000 and 0.000, random interstratification) to phase I (0.027 and 0.045), to phase II (0.054 and 0.090), and finally to sample D (0.083 and 0.135, respectively). Exp layers are randomly distributed in both intermediate phases so that $P_{ExpExp} = W_{Exp}$, $P_{ExpI} = W_I$ and $P_{ExpCh} = W_{Ch}$ as in I-Exp from sample C and in I-Exp-Ch from sample D. Possible mechanisms of the hypothesized solid-state transformation of I-Exp from sample C to I-Exp-Ch from sample D through intermediate I-Exp-Ch phases are detailed in the Appendix.

CONCLUDING REMARKS

A General Pattern for Diagenetic Smectite-to-Illite Transition in Shales

The XRD patterns obtained from the Carter well samples are typical for the diagenetic smectite-to-illite transition (fig. 3). The multi-specimen method led however to an unusual description of the data. In particular, an original clay paragenesis is reported and a novel diagenetic evolution of this paragenesis proposed which includes two stages of smectite illitization.

In the first stage, the clay paragenesis corresponds to the physical mixture of discrete smectite and of a randomly interstratified I-Exp with a high content of illite layers ($W_I > 50\%$) in addition to illite, kaolinite, chlorite and K-Exp. With increasing burial depth, the relative proportion of I-Exp increases, essentially at the expense of discrete smectite, and its composition becomes slightly more illitic. Several conclusions in this study contradict the conventional wisdom of smectite-to-illite transition:

— Smectite illitization is a heterogeneous reaction involving the physical mixture of pure smectite and I-Exp.
— Discrete smectite and I-Exp are authigenic.
— The apparent stability of smectite is higher than commonly assumed as this mineral persists down to 4000 m, although its relative abundance decreases with increasing depth.
— Smectite illitization occurs very early and randomly interstratified I-Exp with $W_I > W_{Exp}$ is formed at shallow burial depth, the temperature at which a I-Exp with a given composition is formed being lower than commonly assumed.
— Smectite illitization rate decreases rapidly, most likely as the result of K-feldspar dissolution.

In the second stage of smectite illitization (below 4000 m depth in the present case study), clay paragenesis consists of two illite-containing mixed layers in addition to illite, kaolinite, chlorite and K-Exp. These two illite-containing mixed layers result from two parallel reaction mechanisms affecting the randomly interstratified I-Exp present in the upper part of the series. The first reaction implies the dissolution of the I-Exp and the crystallization of an ordered I-Exp with R = 1 (MPDO) without significant increase of the I layer content (70% versus 67%, tables 4A, C), possibly as the result of low K-availability. With increasing depth, ordering increases together with a marginal increase of the I layer content (up to 75% in sample F—table 4C). The second reaction affects the remaining fraction of the randomly interstratified I-Exp and implies the polymerization and growth of trioctahedral brucite-like sheets in Exp interlayers, thus developing di-trioctahedral chlorite layers in the initial I-Exp to form a I-Exp-Ch. A possible layer-by-layer mechanism is supported for this reaction by the random layer distribution in the I-Exp-Ch, similar to that of the initial I-Exp. In this scheme, Mg cations released by the dissolution-recrystallization of I-Exp likely represent the Mg source for the formation of brucite-like sheets.

APPENDIX

Single-Phase Segregated I-Exp model: Self-Consistency of the Model

For a given sample, junction probability parameters, P_{ij}, refined for the I-Exp contribution are different for AD and EG states (table 1B). This apparent inconsistency arises from the contrasting expansion behavior of Exp layers in AD and EG states. For example, the hydration behavior of Exp layers is highly heterogeneous in sample A with three types of Exp layers, whereas EG solvation results in the homogeneous swelling of all Exp layers to 16.76 Å (2EG). However, the distribution of illite and expandable layers in I-Exp should be

identical in both states. Therefore, the four-component I-Exp in sample A (AD state) must be reduced to a two-component system following EG solvation if the 15.0, 14.0 and 12.5 Å layers become 2EG layers. To ensure the consistency of the structure model for sample A the sums ($W_{Exp1I} + W_{Exp2I} + W_{Exp3I}$), ($W_{IExp1} + W_{IExp2} + W_{IExp3}$), and ($W_{Exp1Exp1} + W_{Exp1Exp2} + W_{Exp1Exp3} + W_{Exp2Exp1} + W_{Exp2Exp2} + W_{Exp2Exp3} + W_{Exp3Exp1} + W_{Exp3Exp2} + W_{Exp3Exp3}$) obtained for the four-component I-Exp (AD state) must be equal to the parameters W_{ExpI}, W_{IExp} and W_{ExpExp}, respectively, determined for the two-component I-Exp following EG solvation (table 1B). Here, $W_{ij} = W_iP_{ij}$ is the occurrence probability for an ij layer pair (i, j = I, Exp, Exp1, Exp2 and Exp3 − Exp, Exp1, Exp2 and Exp3 denote 16.76, 15.0, 12.5 and 14.0 Å layers). W_{ij} parameters are reported in table A-1 for I-Exp in group I samples. For sample A, $W_{II} = 0.270$ in both AD and EG states and the above relationships are valid. In samples B and C, two types of expandable layers coexist in both AD and EG states. However, the relative amounts of the two types differ in AD and EG states, thus leading to contrasting values of P_{ij} parameters for the corresponding models (table 1B). To ensure the consistency of the proposed models these parameters can be reconciled by considering that some of the expandable layers (noted as Exp′ layers in tables A-1B, C) behave as Exp2 layers in the AD state and as Exp1 layers when EG solvated (tables A-1B, C).

Possible Solid-State Formation of I-Exp-Ch (sample D) at the Expense of I-Exp (Sample C)

As described in the main text, the contents of illite layers in I-Exp from sample C and in I-Exp-Ch from sample D are similar (67 and 70%I, respectively). Junction probability parameters exhibit also strong similarities, interstratification being random in I-Exp from sample C, and showing only slight tendency to segregation in I-Exp-Ch from sample D (table 4). In addition, I-Exp from sample C and I-Exp-Ch from sample D have similar CSD sizes. As a consequence, a solid-state mechanism can be hypothesized for the transition between the two mixed layers, and a series of mixed layers with compositions and structural features (for example the segregation degree of I and Ch Layers, and the random interstratification of Exp layers) intermediate between those of the two end members can be envisaged (table 7). The scope of this section is to describe in detail this hypothesized solid-state transformation and to assess its robustness from the analysis of the relative abundance of layer pairs and triplets (W_{ij}, and W_{ijk}, respectively—i, j, k = I, Exp, Ch) and of their evolution during the transformation. This evolution should follow logically from that of the relative proportion of the different layer types and of their layer stacking.

For this purpose, relative abundances of layer pairs and triplets deduced from structure models (W_{XRD} in table A-2) serve as the basis for this analysis. The first step is thus to calculate the occurrence probabilities for layer pairs and triplets in I-Exp from sample C, in I-Exp-Ch from sample D, and in the two intermediate phases. These occurrence probabilities can be calculated from the junction probabilities listed in table 7 ($W_{ij} = W_iP_{ij}$, and $W_{ijk} = W_{ij}P_{jk}$) and are reported in table A-2 (columns W_{XRD}). The second step is to identify layer pairs whose occurrence probability deduced from structure models (columns W_{XRD}) is decreasing along the reaction pathway (from I-Exp in sample C to phase I to phase II and finally to I-Exp-Ch in sample D). For example, from I-Exp in sample C to phase I, the occurrence probabilities of IExp, ExpI and ExpExp pairs (W_{IExp}, W_{ExpI}, W_{ExpExp}) are decreasing. In table A-2 such pairs are identified with an arrow following their occurrence probability. The third step is to distribute these layer pairs so as to match the occurrence probabilities of layer pairs in the next phase (phase I in our example) as shown in table A-3A. In our example, 0.1798 out of the initial 0.2211 IExp pairs are preserved whereas 0.0319 pairs are transformed to ICh pair, as required for intermediate phase I, the remaining 0.0094 pairs being transformed to II pairs. The same procedure can be applied to ExpI and ExpExp pairs. As a result, theoretical occurrence probabilities can be calculated for all layer pairs in phase I, phase II, and in the I-Exp-Ch from sample D. These values are reported in the W_{Cal} columns of table A-2, and they systematically coincide with W_{XRD} values. The fourth step is to calculate occurrence probabilities for all layer triplets. Again, this starts with the identification of the layer triplets whose occurrence probability deduced from structure models (columns W_{XRD}) is decreasing along the reaction pathway (from I-Exp in sample C to phase I to phase II and finally to I-Exp-Ch in sample D). For example, from I-Exp in sample C to phase I, the occurrence probabilities of IIExp, IExpI, IExpExp, ExpII, ExpIExp, ExpExpI, and ExpExpExp triplets (W_{IIExp}, W_{IExpI}, $W_{IExpExp}$, W_{ExpII}, $W_{ExpIExp}$, $W_{ExpExpI}$, and $W_{ExpExpExp}$) are decreasing. In table A-2 such triplets are identified with an arrow following their occurrence probability. To distribute these "disappearing" layer triplets among newly formed ones, the R = 1 Reichweit parameter implies that the transition probability from one layer pair to another does not depend on the preceding or following layer. As an illustration, one may consider the transformation of the 0.1481 IIExp triplets present in I-Exp from sample C. As IExp pairs may be transformed to II, IExp, and ICh pairs (table A-3A) IIExp triplets are transformed to III, IIExp, and IICh triplets ($0.0063 = 0.1481 \times 0.0094 \div 0.2211$, $0.1204 = 0.1481 \times 0.1798 \div 0.2211$, and $0.0214 = 0.1481 \times 0.0319 \div 0.2211$, respectively). In this case, the initial layer pair (II) is not modified during transformation from I-Exp in sample C to intermediate phase I. If

TABLE A-1A

Single-phase segregated I-Exp model. Relative abundance of the different layer pairs
(W_{ij} parameters) calculated for the segregated I-Exp from sample A

A-AD	I 9.98 Å	Exp1 15.00 Å	Exp2 12.50 Å	Exp3 14.00 Å
I 9.98 Å	0.270	0.060	0.060	0.060
Exp 1 15.00 Å	0.060	0.150	0.050	0.040
Exp2 12.50 Å	0.060	0.050	0.040	0.000
Exp3 14.00 Å	0.060	0.040	0.000	0.000

A-EG	I 9.98 Å	Exp 16.76 Å
I 9.98 Å	0.270	0.180
Exp 16.76 Å	0.180	0.370

Note: The W_{ij} matrices obtained for AD and EG states are equivalent if $Exp_{EG} = Exp1_{AD} + Exp2_{AD} + Exp3_{AD}$.

TABLE A-1B

Single-phase segregated I-Exp model. Relative abundance of the different layer pairs
(W_{ij} parameters) calculated for the segregated I-Exp from sample B

B-AD	I 9.98 Å	Exp1 15.00 Å	Exp2 12.50 Å
I 9.98 Å	0.465	0.116	0.069
Exp1 15.00 Å	0.109	0.074	0.027
Exp2 12.50 Å	0.075	0.021	0.044

B-EG	I 9.98 Å	Exp1 16.76 Å	Exp2 14.00 Å
I 9.98 Å	0.465	0.140	0.044
Exp1 16.76 Å	0.140	0.130	0.000
Exp2 14.00 Å	0.044	0.000	0.036

B	I	Exp1	Exp'	Exp2
I	0.465	0.116	0.025	0.044
Exp1	0.109	0.074	0.027	0.000
Exp'	0.031	0.021	0.008	0.000
Exp2	0.044	0.000	0.000	0.036

Note: The W_{ij} matrices obtained for AD and EG states are equivalent if Exp layers from the present table are combined as follows: $Exp1_{AD} = Exp1$, $Exp2_{AD} = Exp' + Exp2$, $Exp1_{EG} = Exp1 + Exp'$, and $Exp2_{EG} = Exp2$.

TABLE A-1C

Single-phase segregated I-Exp model. Relative abundance of the different layer pairs
(W_{ij} parameters) calculated for the segregated I-Exp from sample C

C-AD	I 9.98 Å	Exp1 15.00 Å	Exp2 12.50 Å	
I 9.98 Å	0.445	0.090	0.116	
Exp1 14.90 Å	0.090	0.023	0.038	
Exp2 12.50 Å	0.116	0.048	0.036	
C-EG	I 9.98 Å	Exp1 16.76 Å	Exp2 14.00 Å	
I 9.98 Å	0.444	0.162	0.044	
Exp1 16.76 Å	0.162	0.108	0.000	
Exp2 14.00 Å	0.044	0.000	0.036	
C	I	Exp1	Exp'	Exp2
I	0.445	0.090	0.072	0.044
Exp1	0.090	0.023	0.038	0.000
Exp'	0.072	0.048	0.000	0.000
Exp2	0.044	0.000	0.000	0.036

Note: The W_{ij} matrices obtained for AD and EG states are equivalent if Exp layers from the present table are combined as follows: $Exp1_{AD}$ = Exp1, $Exp2_{AD}$ = Exp' + Exp2, $Exp1_{EG}$ = Exp1 + Exp', and $Exp2_{EG}$ = Exp2.

both the initial and final layer pairs of a triplet are modified (such as for IExpI triplets from sample C), the two modifications have to be considered separately. Transformation of the first layer pair (IExp) leads to the formation of III, IExpI, and IChI triplets, whereas that of the second layer pair (ExpI) leads to III, IExpI, and IExpCh triplets. Relative proportions of the newly formed layer triplets are calculated as described above [0.0031 = 0.1481 × 0.0094 ÷ (0.2211 + 0.2211), 0.0602 = 0.1481 × 0.1798 ÷ (0.2211 + 0.2211), 0.0214 = 0.1481 × 0.0319 ÷ (0.2211 + 0.2211), 0.0032 = 0.1481 × 0.0095 ÷ (0.2211 + 0.2211), *et cetera*]. These values are reported in table A-3B for all layer triplets and for the different transitions. They can be summed up to calculate theoretical occurrence probabilities for all layer triplets in phase I, phase II, and in the I-Exp-Ch from sample D that are reported in the W_{Cal} columns of table A-2. These values are very similar to those calculated from the XRD structure models determined for I-Exp from sample C and for I-Exp-Ch from sample D, and hypothesized for intermediate phases I and II. Following the transition from I-Exp (sample C) to phase I, differences between W_{Cal} and W_{XRD} are maximum for ExpIExp (0.0115), ChExpI (−0.0080), IExpExp (0.0074), and ExpExpI (0.0069) triplets. For the phase I to phase II transition, these differences are most substantial for ExpIExp (0.0085) and ExpExpI (0.0061) triplets. For the transition from phase II to I-Exp-Ch (sample D), only IChCh and ChChI layer triplets present non-negligible differences between the W_{Cal} and W_{XRD} (−0.0079, and −0.0065, respectively). Overall, the observed agreement between calculated W_{ijk} values and those derived from structure models is excellent and supports the hypothesized solid-state reaction mechanism as it is strongly influenced by the choice of junction probability parameters. In particular, if the P_{SS} = W_S is not maintained for intermediate phases, calculated W_{ijk} values differ significantly from those derived from structure models. However, I-Exp-Ch structure models hypothesized for intermediate phases I and II and layer pair transitions are to be considered only as an approximation to the actual mechanism of I-Exp-Ch formation at the expense of I-Exp.

TABLE A-2

Relative abundance of layers, layer pairs and triplets determined for the hypothesized solid-state transformation transition between the IExp phase from sample C and the I-Exp-Ch phase from sample D

Layer Sequence	Sample C W_{XRD}	Inter. phase I W_{Cal}	Inter. phase I W_{XRD}	Inter. phase II W_{Cal}	Inter. phase II W_{XRD}	Sample D W_{Cal}	Sample D W_{XRD}
				Samples			
I	0.67	0.68	0.68	0.69	0.69	0.70	0.70
Exp	0.33 →	0.27	0.27 →	0.21	0.21 →	0.15	0.15
Ch	0.00	0.05	0.05	0.10	0.10	0.15	0.15
II	0.4489	0.4684	0.4684	0.4879	0.4878	0.5072	0.5072
IExp	0.2211 →	0.1798	0.1798 →	0.1413	0.1413 →	0.1050	0.1050
ICh	0.0000	0.0319	0.0319	0.0609	0.0609	0.0878	0.0878
ExpI	0.2211 →	0.1836	0.1836 →	0.1449	0.1449 →	0.1050	0.1050
ExpExp	0.1089 →	0.0729	0.0729 →	0.0441	0.0441 →	0.0225	0.0225
ExpCh	0.0000	0.0135	0.0135	0.0210	0.0210	0.0225	0.0225
ChI	0.000	0.0280	0.0280	0.0573	0.0573	0.0878	0.0878
ChExp	0.000	0.0173	0.0173	0.0246	0.0246 →	0.0225	0.0225
ChCh	0.000	0.0046	0.0046	0.0181	0.0181	0.0397	0.0398
III	0.3008	0.3200	0.3226	0.3424	0.3449	0.3647	0.3676
IIExp	0.1481 →	0.1241	0.1238 →	0.1007	0.0999 →	0.0768	0.0761
IICh	0.0000	0.0214	0.0219	0.0419	0.0430	0.0621	0.0636
IExpI	0.1481 →	0.1217	0.1223 →	0.0958	0.0975 →	0.0716	0.0735
IExpExp	0.0730 →	0.0559	0.0485 →	0.0356	0.0297 →	0.0204	0.0158
IExpC	0.0000	0.0030	0.0090	0.0104	0.0141	0.0143	0.0158
IChI	0.0000	0.0201	0.0179	0.0374	0.0349	0.0545	0.0513
IChExp	0.0000	0.0109	0.0110	0.0180	0.0150 →	0.0180	0.0132
IChCh	0.0000	0.0010	0.0030	0.0056	0.0110	0.0154	0.0233
ExpII	0.1481 →	0.1267	0.1265 →	0.1032	0.1024 →	0.0768	0.0761
ExpIExp	0.0730 →	0.0600	0.0485 →	0.0382	0.0297 →	0.0218	0.0158
ExpICh	0.0000	0.0053	0.0086	0.0125	0.0128	0.0156	0.0132
ExpExpI	0.0730 →	0.0567	0.0496 →	0.0365	0.0304 →	0.0205	0.0158
ExpExpExp	0.0359 →	0.0240	0.0197 →	0.0120	0.0093 →	0.0048	0.0034
ExpExpCh	0.0000	0.0022	0.0036	0.0046	0.0044 →	0.0024	0.0034
ExpChI	0.0000	0.0091	0.0076	0.0147	0.0120	0.0169	0.0132
ExpChExp	0.0000	0.0051	0.0047	0.0067	0.0052 →	0.0050	0.0034
ExpChCh	0.0000	0.0008	0.0013	0.0031	0.0038	0.0064	0.0060
ChII	0.0000	0.0188	0.0193	0.0395	0.0405	0.0630	0.0636
ChIExp	0.0000	0.0046	0.0074	0.0113	0.0117	0.0149	0.0132
ChICh	0.0000	0.0000	0.0013	0.0013	0.0051	0.0051	0.0110
ChExpI	0.0000	0.0038	0.0118	0.0132	0.0170 →	0.0130	0.0158
ChExpExp	0.0000	0.0029	0.0047	0.0057	0.0052 →	0.0034	0.0034
ChExpCh	0.0000	0.0000	0.0009	0.0009	0.0025	0.0026	0.0034
ChChI	0.0000	0.0010	0.0026	0.0052	0.0104	0.0168	0.0233
ChChExp	0.0000	0.0008	0.0016	0.0034	0.0045	0.0068	0.0060
ChChCh	0.0000	0.0000	0.0004	0.0004	0.0033	0.0068	0.0105

Note: W_{XRD} values are deduced directly from the structure model determined from I-Exp in sample C and for I-Exp-Ch in sample D. For the theoretical phase I and II, W_{XRD} values are deduced from the hypothesized structure models intermediate between the two end-members (see text for details). W_{Cal} values are calculated assuming the redistribution of layers, layer pairs and triplets whose relative proportion is decreasing from one step to the next one. These layers, layer pairs and triplets are indicated by arrows in the present table. Redistribution of these layers, layer pairs and triplets is described in table A-3.

<div align="center">

Table A-3A

Redistribution of layer pairs whose relative proportion is decreasing from one step to the next one during the hypothesized solid-state transformation transition between the I-Exp phase in sample C and the I-Exp-Ch phase in sample D

</div>

I-Exp in sample C		Phase I	
0.2211	IExp	II	0.0094
		IExp	0.1798
		ICh	0.0319
0.2211	ExpI	II	0.0095
		ExpI	0.1836
		ChI	0.0280
0.1089	ExpExp	II	0.0006
		ExpCh	0.0135
		ExpExp	0.0729
		ChExp	0.0173
		ChCh	0.0046

Note: Layer pairs whose proportion is stable or increasing during any of the three steps are not reported in the present table. Their relative abundances, reported in table A-2, are calculated as the sum of their relative abundance in the previous reaction step and of the present redistribution.

Phase I		Phase II	
0.1798	IExp	II	0.0095
		IExp	0.1413
		ICh	0.0290
0.1836	ExpI	II	0.0095
		ExpI	0.1449
		ChI	0.0292
0.0729	ExpExp	II	0.0005
		ExpCh	0.0075
		ExpExp	0.0441
		ChExp	0.0073
		ChCh	0.0135

Phase II		I-Exp in sample D	
0.1413	IExp	II	0.0094
		IExp	0.1050
		ICh	0.0269
0.1449	ExpI	II	0.0094
		ExpI	0.1050
		ChI	0.0305
0.0441	ExpExp	II	0.0006
		ExpCh	0.0015
		ExpExp	0.0225
		ChCh	0.0195
0.0246	ChExp	ChExp	0.0225
		ChCh	0.0021

Table A-3B

Redistribution of layer triplets whose relative proportion is decreasing from one step to the next one during the hypothesized solid-state transformation transition between the I-Exp phase in sample C and the I-Exp-Ch phase in sample D

I-Exp in sample C		⟹	Phase I	
			III	0.0063
0.1481	IIExp		IIExp	0.1204
			IICh	0.0214
			III	0.0031
			IExpI	0.0602
0.1481	IExpI		IChI	0.0107
			III	0.0032
			IExpI	0.0615
			IChI	0.0094
			IIExp	0.0021
			IExpExp	0.0398
			IChExp	0.0071
0.0730	IExpExp		III	0.0001
			IExpCh	0.0030
			IExpExp	0.0161
			IChExp	0.0038
			IChCh	0.0010
			III	0.0064
0.1481	ExpII		ExpII	0.1230
			ChII	0.0188
			IIExp	0.0016
			ExpIExp	0.0303
0.0730	ExpIExp		ChIExp	0.0046
			ExpII	0.0016
			ExpIExp	0.0297
			ExpICh	0.0053
			III	0.0001
			ExpChI	0.0029
			ExpExpI	0.0161
			ChExpI	0.0038
0.0730	ExpExpI		ChChI	0.0010
			ExpII	0.0021
			ExpExpI	0.0406
			ExpChI	0.0062
			ExpChExp	0.0022
			ExpExpExp	0.0120
			ChExpExp	0.0029
			ChChExp	0.0008
0.0359	ExpExpExp		ExpExpCh	0.0022
			ExpExpExp	0.0120
			ExpChExp	0.0029
			ExpChCh	0.0008

TABLE A-3B

(continued)

Phase I		Phase II	
0.1241	IIExp	III	0.0066
		IIExp	0.0975
		IICh	0.0200
0.1217	IExpI	III	0.0032
		IExpI	0.0473
		IChI	0.0097
		III	0.0032
		IExpI	0.0485
		IChI	0.0098
0.0485	IExpExp	IIExp	0.0018
		IExpExp	0.0271
		IChExp	0.0056
		III	0.0001
		IExpCh	0.0014
		IExpExp	0.0085
		IChExp	0.0014
		IChCh	0.0026
0.1267	ExpII	III	0.0066
		ExpII	0.1000
		ChII	0.0202
0.0485	ExpIExp	IIExp	0.0013
		ExpIExp	0.0189
		ChIExp	0.0039
		ExpII	0.0013
		ExpIExp	0.0193
		ExpICh	0.0039
0.0496	ExpExpI	III	0.0001
		ExpChI	0.0015
		ExpExpI	0.0085
		ChExpI	0.0014
		ChChI	0.0026
		ExpII	0.0018
		ExpExpI	0.0280
		ExpChI	0.0056
0.0197	ExpExpExp	IIExp	0.0001
		ExpChExp	0.0010
		ExpExpExp	0.0060
		ChExpExp	0.0010
		ChChExp	0.0018
		ExpII	0.0001
		ExpExpCh	0.0010
		ExpExpExp	0.0060
		ExpChExp	0.0010
		ExpChCh	0.0018

<div align="center">

T<small>ABLE</small> A-3B

(continued)

</div>

Phase II		⟹	I-Exp-Ch in sample D	
			III	0.0066
0.0999	IIExp		IIExp	0.0742
			IICh	0.0190
			III	0.0032
			IExpI	0.0358
0.0975	IExpI		IChI	0.0092
			III	0.0032
			IExpI	0.0358
			IChI	0.0104
			IIExp	0.0015
			IExpExp	0.0168
			IChExp	0.0043
0.0297	IExpExp		III	0.0001
			IExpCh	0.0002
			IExpExp	0.0036
			IChCh	0.0031
0.0150	IChExp		IChExp	0.0137
			IChCh	0.0013
			III	0.0066
0.1024	ExpII		ExpII	0.0743
			ChII	0.0216
			IIExp	0.0010
			ExpIExp	0.0109
0.0297	ExpIExp		ChIExp	0.0032
			ExpII	0.0010
			ExpIExp	0.0109
			ExpICh	0.0028
			III	0.0001
			ExpExpI	0.0036
			ChExpI	0.0002
0.0304	ExpExpI		ChChI	0.0031
			ExpII	0.0015
			ExpExpI	0.0169
			ExpChI	0.0049
			IIExp	0.0001
			ExpChExp	0.0002
			ExpExpExp	0.0024
0.0093	ExpExpExp		ChChExp	0.0021
			ExpII	0.0001
			ExpExpCh	0.0002
			ExpExpExp	0.0024
			ExpChCh	0.0021

TABLE A-3B

(continued)

Phase II		⟹	I-Exp-Ch in sample D	
			IICh	0.0002
0.0150	ExpExpCh		ExpExpCh	0.0077
			ExpChCh	0.0005
			ChChCh	0.0066
0.0052	ExpChExp		ExpChExp	0.0048
			ExpChCh	0.0004
			ChExpI	0.0023
			ChChI	0.0002
0.0170	ChExpI		ChII	0.0009
			ChExpI	0.0105
			ChChI	0.0031
			ChExpExp	0.0017
			ChChExp	0.0002
0.0052	ChExpExp		ChII	0.0000
			ChExpExp	0.0017
			ChExpCh	0.0001
			ChChCh	0.0015

Note: The redistribution of layer triplets among newly formed ones is done assuming that the transition probability from one layer pair to another does not depend on the preceding or following layer as R = 1 (see text for details). Layer triplets whose proportion is stable or increasing during any of the three steps are not reported in the present table. Their relative abundances, reported in table A-2, are calculated as the sum of their relative abundance in the previous reaction step and of the present redistribution. 67
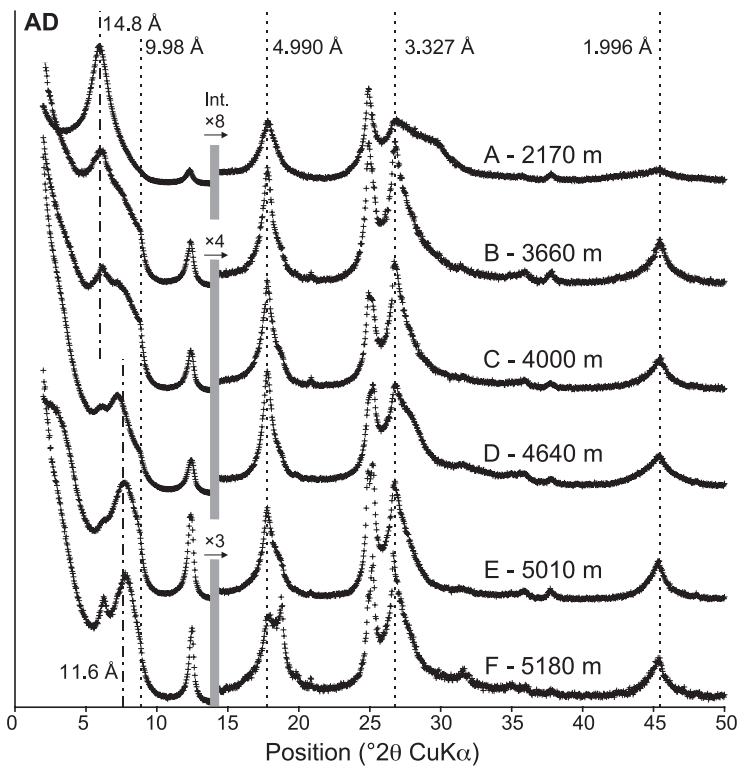
Fig. A-1. Experimental XRD patterns obtained from Carter well samples selected as being representative of the complete smectite-to-illite diagenetic transition. Sampling depths are 2170 (A), 3660 (B), 4000 (C), 4640 (D), 5010 (E), and 5180 m (F). Data collected on air dried samples at 40% relative humidity. Patterns as in figure 1.
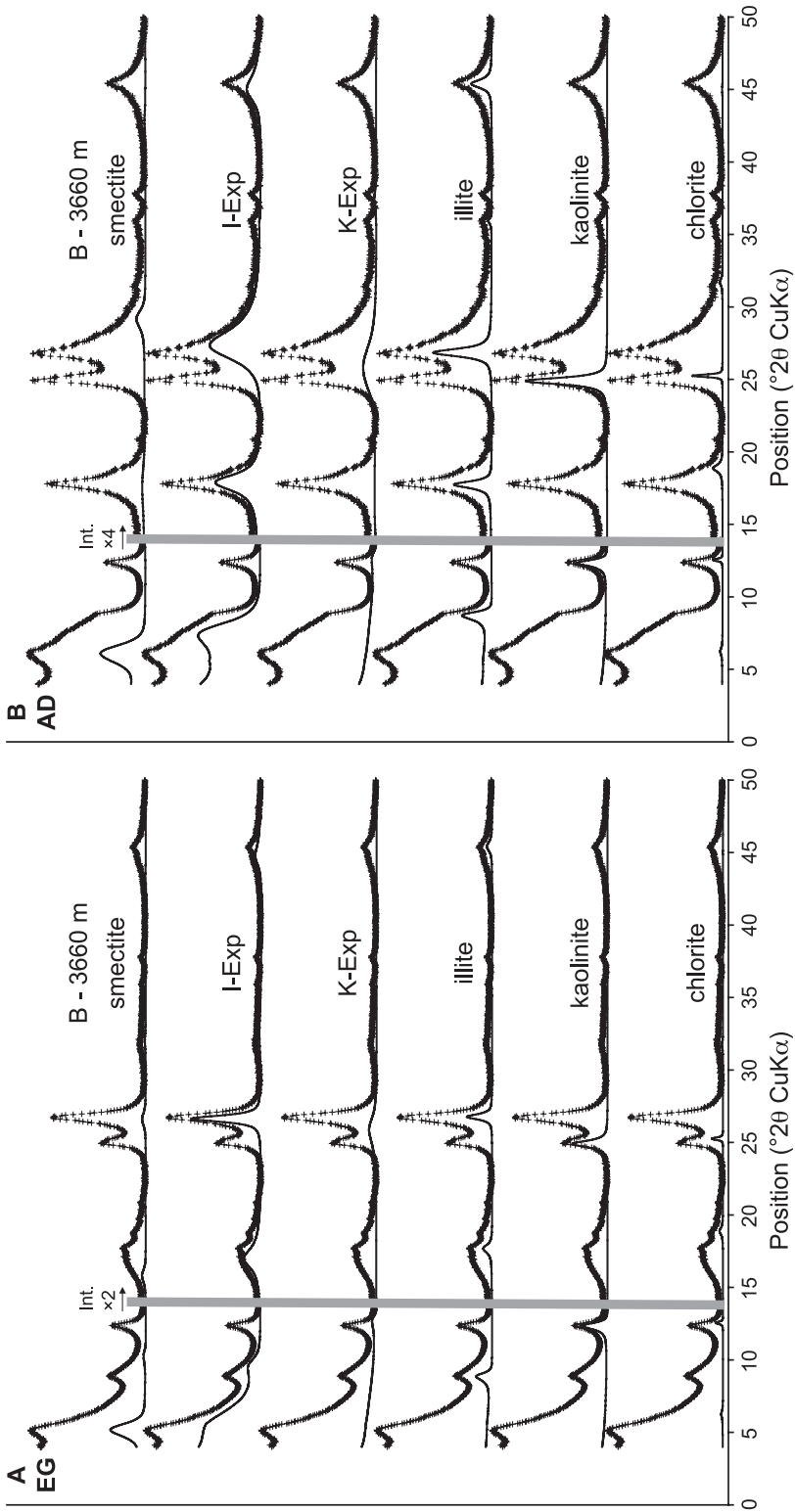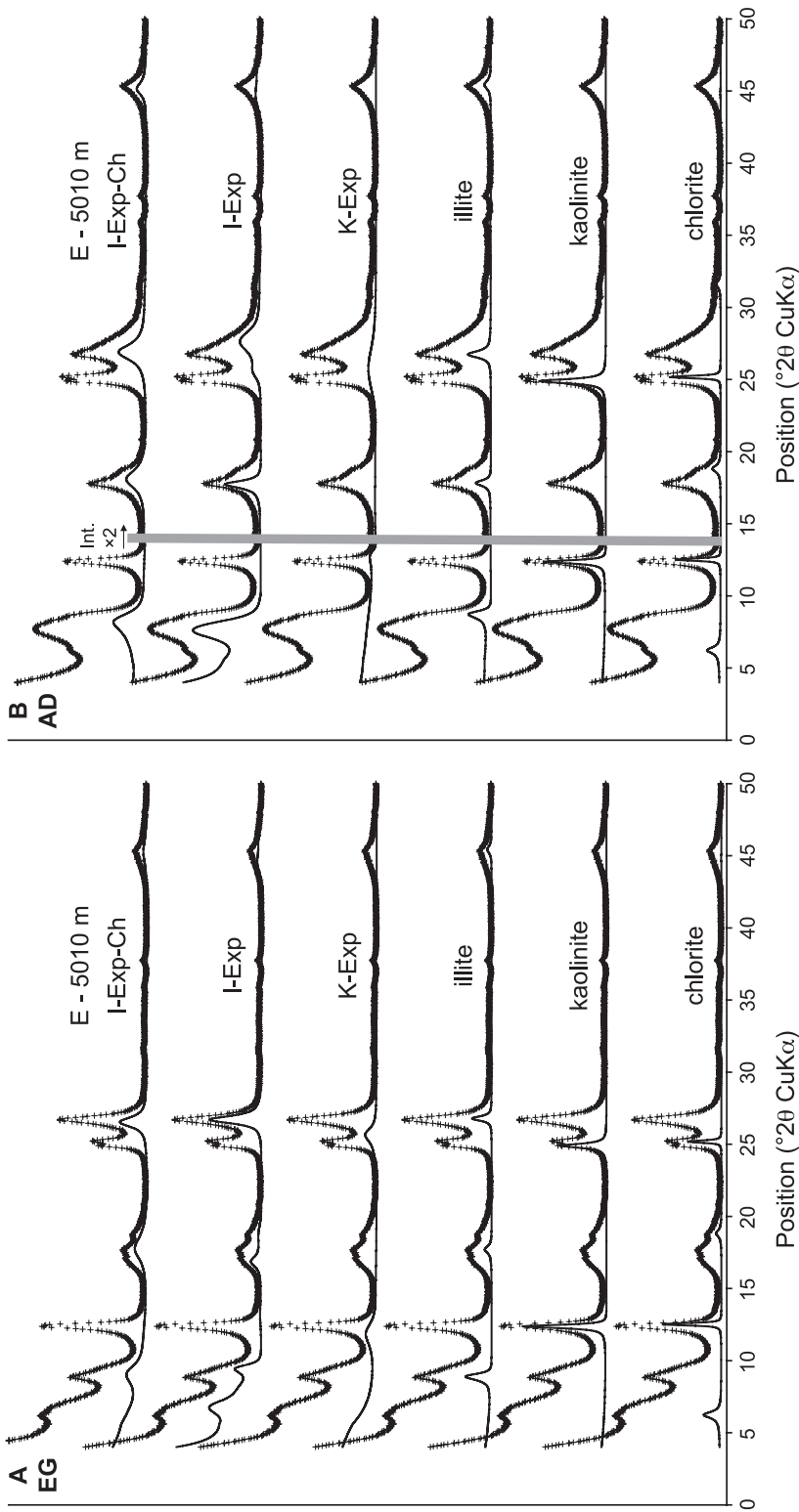
Fig. A-2. Elementary contributions to the intensity diffracted by sample B (3660 m). Patterns as for figure 5. The structural parameters for the optimal models are given in table 4A. (A). EG solvated sample. (B). Air-dried sample.

Fig. A-3. Elementary contributions to the intensity diffracted by sample E (5010 m). Patterns as for figure 5. The structural parameters for the optimal models are given in table 4C. (A). Air-dried sample. (B). EG solvated sample.
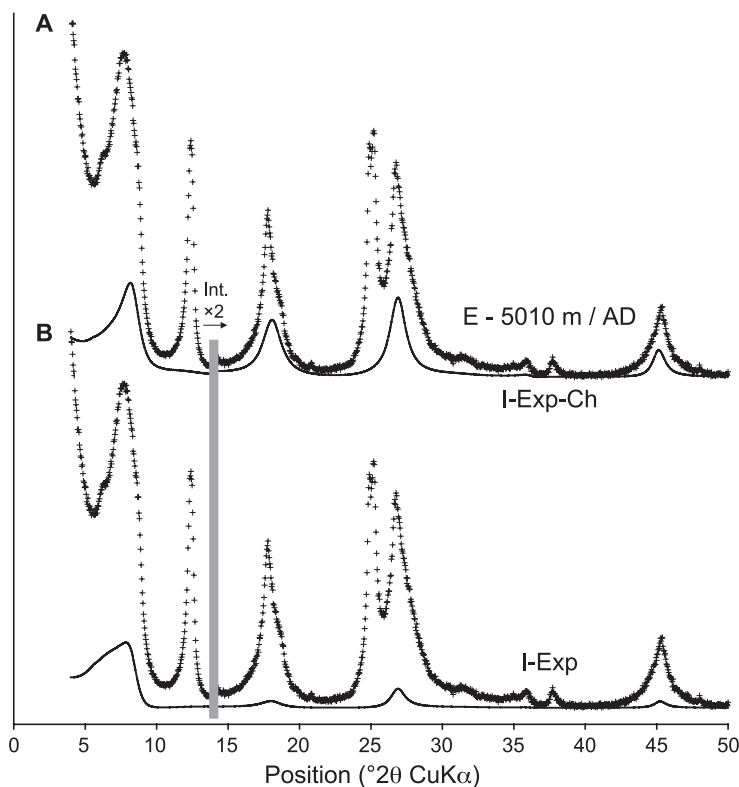
Fig. A-4. Sensitivity of calculated XRD patterns to structural parameters. Patterns as for figure 5. (A). Sample E—5010 m Ca-saturated air-dried. Elementary contribution of the optimum I-Exp-Ch (table 4C). (B). Sample E—5010 m Ca-saturated air-dried. 14.0 Å Ch layers (with 3.0 Mg and 6.0 OH per half unit-cell in their interlayers) of the optimum I-Exp-Ch are replaced by 14.0 Å Exp layers (with 0.25 Mg and 2.0 OH per half unit-cell in their interlayers).

REFERENCES

Altaner, S. P., and Ylagan, R. F., 1997, Comparison of structural models of mixed-layer illite/smectite and reaction mechanisms of smectite illitization: Clays and Clay Minerals, v. 45, p. 517–533, doi:10.1346/CCMN.1997.0450404.

Altaner, S. P., Ylagan, R. F., Savin, S. M., Aronson, J. L., Belkin, H. E., and Pozzuoli, A., 2003, Geothermometry, geochronology, and mass transfer associated with hydrothermal alteration of a rhyolitic hyaloclastite from Ponza Island, Italy: Geochimica et Cosmochimica Acta, v. 67, p. 275–288, doi:10.1016/S0016-7037(02)01077-3.

Aplin, A. C., Matenaar, I. F., McCarty, D. K., and van Der Pluijm, B. A., 2006, Influence of mechanical compaction and clay mineral diagenesis on the microfabric and pore-scale properties of deep-water Gulf of Mexico Mudstones: Clays and Clay Minerals, v. 54, p. 500–514, doi:10.1346/CCMN.2006.0540411.

Aronson, J. L., and Hower, J., 1976, Mechanism of burial metamorphism of argillaceous sediments: 2. Radiogenic argon evidence: Geological Society of America Bulletin, v. 87, p. 738–744, doi:10.1130/0016-7606(1976)87⟨738:MOBMOA⟩2.0.CO;2.

Bauer, A., and Velde, B., 1999, Smectite transformation in high molar KOH solutions: Clay Minerals, v. 34, p. 259–273, doi:10.1180/000985599546226.

Berger, G., Velde, B., and Aigouy, T., 1999, Potassium sources and illitization in Texas Gulf Coast shale diagenesis: Journal of Sedimentary Research, v. 69, p. 151–157.

Bethke, C. M., and Altaner, S. P., 1986, Layer-by-layer mechanism of smectite illitization and application to a new rate law: Clays and Clay Minerals, v. 34, p. 136–145, doi:10.1346/CCMN.1986.0340204.

Bethke, C. M., Vergo, N., and Altaner, S. P., 1986, Pathways of smectite illitization: Clays and Clay Minerals, v. 34, p. 125–135, doi:10.1346/CCMN.1986.0340203.

Billault, V., Beaufort, D., Patrier, P., and Petit, S., 2002, Crystal chemistry of Fe-sudoites from Uranium deposits in the Athabasca basin (Saskatchewan, Canada): Clays and Clay Minerals, v. 50, p. 70–81, doi:10.1346/000986002761002847.

Boles, J. R., and Francks, G. S., 1979, Clay diagenesis in Wilcox sandstones of Southwest Texas: Implications of smectite diagenesis on sandstone cementation: Journal of Sedimentary Petrology, v. 49, p. 55–70.

Brindley, G. W., Suzuki, T., and Thiry, M., 1983, Interstratified kaolinite/smectites from the Paris Basin; correlations of layer proportions, chemical compositions and other data: Bulletin de Minéralogie, v. 106, p. 403–410.

Burst, J. F., 1957, Postdiagenetic clay mineral environmental relationships in the Gulf Coast Eocene: Clays and Clay Minerals, v. 6, p. 327–341, doi:10.1346/CCMN.1957.0060124.

——— 1969, Diagenesis of Gulf Coast clayey sediments and its possible relation to petroleum migration: American Association of Petroleum Geologists Bulletin, v. 53, p. 73–93.

Chen, Z. S., Tsou, T. C., Asio, V. B., and Tsai, C. C., 2001, Genesis of inceptisols on a volcanic landscape in Taiwan: Soil Science, v. 166, p. 255–266.

Claret, F., ms, 2001, Caractérisation structurale des transitions minéralogiques dans les formations argileuses: Contrôles et implications géochimiques des processus d'illitisation. Cas particulier d'une perturbation alcaline dans le Callovo-Oxfordien Laboratoire souterrain Meuse-Haute-Marne: Environmental and Geochimistry Group, Grenoble, France, Université Joseph Fourrier, Ph. D. thesis, 174 p.

Claret, F., Sakharov, B. A., Drits, V. A., Velde, B., Meunier, A., Griffault, L., and Lanson, B., 2004, Clay minerals in the Meuse-Haute Marne underground laboratory (France): Possible influence of organic matter on clay mineral evolution: Clays and Clay Minerals, v. 52, p. 515–532.

Dong, H., 2005, Interstratified illite-smectite: A review of contributions of TEM data to crystal chemical relations and reaction mechanisms: Clay Science, v. 12, Supplement 1, p. 6–12.

Dong, H., Peacor, D. R., and Freed, R. L., 1997, Phase relations among smectite, R1 illite-smectite, and illite: American Mineralogist, v. 82, p. 379–391.

Douglas, L. A., 1989, Vermiculites, *in* Dixon, J. B., and Weed, S. B., editors, Minerals in Soil Environments: Madison, Wisconsin, Soil Science Society of America Book Series 1, p. 635–728.

Drits, V. A., and Sakharov, B. A., 1976, X-Ray structural analysis of mixed-layer minerals: Moscow, Nauka, Transactions of the Academy of Sciences U.S.S.R., v. 295, 256 p.

Drits, V. A., and Tchoubar, C., 1990, X-ray diffraction by disordered lamellar structures: Theory and applications to microdivided silicates and carbons: Berlin, Springer-Verlag, 371 p.

Drits, V. A., Varaxina, T. V., Sakharov, B. A., and Plançon, A., 1994, A simple technique for identification of one-dimensional powder X-ray diffraction patterns for mixed-layer illite-smectites and other interstratified minerals: Clays and Clay Minerals, v. 42, p. 382–390.

Drits, V. A., Sakharov, B. A., Lindgreen, H., and Salyn, A. L., 1997a, Sequential structure transformation of illite-smectite-vermiculite during diagenesis of Upper Jurassic shales from the North Sea and Denmark: Clay Minerals, v. 32, p. 351–371.

Drits, V. A., Srodon, J., and Eberl, D. D., 1997b, XRD measurement of mean crystallite thickness of illite and illite/smectite: Reappraisal of the Kubler index and the Scherrer equation: Clays and Clays Minerals, v. 45, p. 461–475.

Drits, V. A., Lindgreen, H., Sakharov, B. A., Jakobsen, H. J., Salyn, A. L., and Dainyak, L. G., 2002a, Tobelitization of smectite during oil generation in oil-source shales. Application to North Sea illite-tobelite-smectite-vermiculite: Clays and Clay Minerals, v. 50, p. 82–98.

Drits, V. A., Sakharov, B. A., Dainyak, L. G., Salyn, A. L., and Lindgreen, H., 2002b, Structural and chemical heterogeneity of illite-smectites from Upper Jurassic mudstones of East Greenland related to volcanic and weathered parent rocks: American Mineralogist, v. 87, p. 1590–1606.

Drits, V. A., Lindgreen, H., Sakharov, B. A., Jakobsen, H. J., and Zviagina, B. B., 2004, The detailed structure and origin of clay minerals at the Cretaceous/Tertiary boundary, Stevns Klint (Denmark): Clay Minerals, v. 39, p. 367–390.

Drits, V. A., Lindgreen, H., Sakharov, B. A., Jakobsen, H. J., Fallick, A. E., Salyn, A. L., Dainyak, L. G., Zviagina, B. B., and Barfod, D. N., 2007, Formation and transformation of mixed-layer minerals by Tertiary intrusives in Cretaceous mudstones, West Greenland: Clays and Clay Minerals, v. 55, p. 260–283.

Ferrage, E., Lanson, B., Malikova, N., Plancon, A., Sakharov, B. A., and Drits, V. A., 2005a, New Insights on the Distribution of Interlayer Water in Bi-Hydrated Smectite from X-ray Diffraction Profile Modeling of 00l Reflections: Chemistry of Materials, v. 17, p. 3499–3512, doi: 10.1021/cm047995v.

Ferrage, E., Lanson, B., Sakharov, B. A., and Drits, V. A., 2005b, Investigation of smectite hydration properties by modeling experimental X-ray diffraction patterns: Part I. Montmorillonite hydration properties: American Mineralogist, v. 90, p. 1358–1374, doi:10.2138/am.2005.1776.

Ferrage, E., Lanson, B., Sakharov, B. A., Geoffroy, N., Jacquot, E., and Drits, V. A., 2007, Investigation of dioctahedral smectite hydration properties by modeling of X-ray diffraction profiles: Influence of layer charge and charge location: American Mineralogist, v. 92, p. 1731–1743, doi:10.2138/am.2007.2273.

Freed, R. L., and Peacor, D. R., 1992, Diagenesis and the formation of authigenic illite-rich I/S crystals in Gulf Coast shales: TEM study of clay separates: Journal of Sedimentary Petrology, v. 62, p. 220–234.

Hoffman, J., and Hower, J., 1979, Clay mineral assemblages as low grade metamorphic geothermometers: Application to the thrust faulted disturbed belt of Montana, U.S.A., *in* Scholle, P. A., and Schluger, R. P., editors, Aspects of Diagenesis: Tulsa, Oklahoma, SEPM Special Publication n. 26, p. 55–79.

Howard, S. A., and Preston, K. D., 1989, Profile fitting of powder diffraction patterns, *in* Bish, D. L., and Post, J. E., editors, Modern Powder Diffraction: Washington D.C., Mineralogical Society of America, Reviews in Mineralogy, v. 20, p. 217–275.

Hower, J., Eslinger, E. V., Hower, M. E., and Perry, E. A., 1976, Mechanism of burial metamorphism of argillaceous sediment: 1. Mineralogical and chemical evidence: Geological Society of America Bulletin, v. 87, p. 725–737, doi:10.1130/0016-7606(1976)87⟨725:MOBMOA⟩2.0.CO;2.

Huang, W. L., 1993, The formation of illitic clays from kaolinite in KOH solution from 225°C to 350°C: Clays and Clay Minerals, v. 41, p. 645–654, doi:10.1346/CCMN.1993.0410602.

Inoue, A., and Utada, M., 1983, Further investigations of a conversion series of dioctahedral mica/smectites in the Shinzan hydrothermal alteration area, northeast Japan: Clays and Clay Minerals, v. 31, p. 401–412, doi:10.1346/CCMN.1983.0310601.

Inoue, A., Minato, H., and Utada, M., 1978, Mineralogical properties and occurrence of illite/montmorillonite mixed layer minerals formed from Miocene volcanic glass in Waga-Omono district: Clay Science, v. 5, p. 123–136.

Inoue, A., Velde, B., Meunier, A., and Touchard, G., 1988, Mechanism of illite formation during smectite-to-illite conversion in a hydrothermal system: American Mineralogist, v. 73, p. 1325–1334.

Inoue, A., Bouchet, A., Velde, B., and Meunier, A., 1989, Convenient technique for estimating smectite layer percentage in randomly interstratified illite/smectite minerals: Clays and Clay Minerals, v. 37, p. 227–234, doi:10.1346/CCMN.1989.0370305.

Inoue, A., Watanabe, T., Kohyama, N., and Brusewitz, A. M., 1990, Characterization of illitization of smectite in bentonite beds at Kinnekulle, Sweden: Clays and Clay Minerals, v. 38, p. 241–249, doi:10.1346/CCMN.1990.0380302.

Inoue, A., Lanson, B., Marques-Fernandes, M., Sakharov, B. A., Murakami, T., Meunier, A., and Beaufort, D., 2005, Illite-smectite mixed-layer minerals in the hydrothermal alteration of volcanic rocks: I. One-dimensional XRD structure analysis and characterization of component layers: Clays and Clay Minerals, v. 53, p. 423–439, doi:10.1346/CCMN.2005.0530501.

Jagodzinski, H., 1949, Eindimensionale Fehlordnung in Kristallen und ihr Einfluss auf die Röntgeninterferenzen: I. Berechnung des Fehlordnungsgrades aus der Röntgenintensitaten: Acta Crystallographica, v. 2, p. 201–207, doi:10.1107/S0365110X49000552.

Jennings, S., and Thompson, G. R., 1986, Diagenesis of Plio-Pleistocene sediments of the Colorado River delta, southern California: Journal of Sedimentary Petrology, v. 56, p. 89–98.

Kameda, J., Miyawaki, R., Kitagawa, R., and Kogure, T., 2007, XRD and HRTEM analyses of stacking structures in sudoite, di-trioctahedral chlorite: American Mineralogist, v. 92, p. 1586–1592, doi:10.2138/am.2007.2410.

Lanson, B., 2005, Crystal structure of mixed-layer minerals and their X-ray identification: New insights from X-ray diffraction profile modeling: Clay Science, v. 12, Supplement 1, p. 1–5.

Lanson, B., Sakharov, B. A., Claret, F., and Drits, V. A., 2005, Diagenetic evolution of clay minerals in Gulf Coast shales: New insights from X-ray diffraction profile modeling: Burlington, Vermont, 42nd Annual Meeting, Clay Minerals Society, p. 69.

Li, G., Peacor, D. R., and Coombs, D. S., 1997, Transformation of smectite to illite in bentonite and associated sediments from Kaka point, New Zealand: Contrast in rate and mechanism: Clays and Clay Minerals, v. 45, p. 54–67, doi:10.1346/CCMN.1997.0450106

Lin, C. Y., and Bailey, S. W., 1985, Structural data for sudoite: Clays and Clay Minerals, v. 33, p. 410–414, doi:10.1346/CCMN.1985.0330506.

Lindgreen, H., Drits, V. A., Sakharov, B. A., Salyn, A. L., Wrang, P., and Dainyak, L. G., 2000, Illite-smectite structural changes during metamorphism in black Cambrian Alum shales from the Baltic area: American Mineralogist, v. 85, p. 1223–1238.

Lindgreen, H., Drits, V. A., Sakharov, B. A., Jakobsen, H. J., Salyn, A. L., Dainyak, L. G., and Kroyer, H., 2002, The structure and diagenetic transformation of illite-smectite and chlorite-smectite from North Sea Cretaceous-Tertiary chalk: Clay Minerals, v. 37, p. 429–450, doi: 10.1180/0009855023730055.

Marques, J. J., Teixeira, W. G., Schulze, D. G., and Curi, N., 2002, Mineralogy of soils with unusually high exchangeable Al from the western Amazon Region: Clay Minerals, v. 37, p. 651–661, doi: 10.1180/0009855023740067.

McCarty, D. K., 2005, XRD pattern simulation of clays and geological interpretation: Burlington, Vermont, 42nd Annual Meeting, The Clay Minerals Society, Program and Abstracts, p. 78.

McCarty, D. K., Drits, V. A., Sakharov, B., Zviagina, B. B., Ruffell, A., and Wach, G., 2004, Heterogeneous mixed-layer clays from the Cretaceous greensand, Isle of Wight, southern England: Clays and Clay Minerals, v. 52, p. 552–575, doi: 10.1346/CCMN.2004.0520505.

McCarty, D. K., Drits, V. A., and Sakharov, B. A., 2005, Advantages and limitations of simulation of XRD patterns of clays: Mod-1 to present: Burlington, Vermont, 42nd Annual Meeting, The Clay Minerals Society, Program and Abstracts, p. 76.

McCarty, D. K., Sakharov, B. A., and Drits, V. A., 2008, Early clay diagenesis in Gulf Coast sediments: New insights from XRD profile modeling: Clays and Clay Minerals, v. 56, p. 359–379, doi: 10.1346/CCMN.2008.0560306.

Méring, J., 1949, L'interférence des rayons-X dans les systèmes à stratification désordonnée: Acta Crystallographica, v. 2, p. 371–377, doi:10.1107/S0365110X4900097.

Moore, D. M., and Reynolds, R. C., Jr., 1997, X-ray Diffraction and the Identification and Analysis of Clay Minerals: United Kingdom, Oxford University Press, 378 p.

Nadeau, P. H., and Reynolds, R. C., Jr., 1981, Burial and contact metamorphism in the Mancos Shale: Clays and Clay Minerals, v. 29, p. 249–259.

Perry, E. A., and Hower, J., 1970, Burial diagenesis in Gulf Coast pelitic sediments: Clays and Clay Minerals, v. 18, p. 165–177, doi: 10.1346/CCMN.1970.0180306.

—— 1972, Late-stage dehydration in deeply buried pelitic sediments: American Association of Petroleum Geologists Bulletin, v. 56, p. 2013–2021.

Pytte, A. M., and Reynolds, R. C., 1989, The thermal transformation of smectite to illite, *in* Naeser, N. D., and McCulloh, T. H., editors, Thermal History of Sedimentary Basins: Methods and Case Histories: New York, Springer, p. 133–140.

Reynolds, R. C., Jr., 1967, Interstratified clay systems: Calculation of the total one-dimensional diffraction function: American Mineralogist, v. 52, p. 661–672.

—— 1980, Interstratified clay minerals, *in* Brindley, G. W., and Brown, G., editors, Crystal structures of clay

minerals and their X-ray identification: London, The Mineralogical Society, Monograph n. 5, p. 249–359.

—— 1986, The Lorentz-polarization factor and preferred orientation in oriented clay aggregates: Clays and Clay Minerals, v. 34, p. 359–367.

Reynolds, R. C., Jr., and Hower, J., 1970, The nature of interlayering in mixed-layer illite-montmorillonites: Clays and Clay Minerals, v. 18, p. 25–36, doi: 10.1346/CCMN.1970.0180104.

Sakharov, B. A., and Drits, V. A., 1973, Mixed-layer kaolinite-montmorillonite: A comparison of observed and calculated diffraction patterns: Clays and Clay Minerals, v. 21, p. 15–17, doi: 10.1346/CCMN.1973.0210104.

Sakharov, B. A., Lindgreen, H., Salyn, A. L., and Drits, V. A., 1999a, Mixed-layer kaolinite-illite-vermiculite in North Sea shales: Clay Minerals, v. 34, p. 333–344.

—— 1999b, Determination of illite-smectite structures using multispecimen X-ray diffraction profile fitting: Clays and Clays Minerals, v. 47, p. 555–566.

Sakharov, B. A., Dubinska, E., Bylina, P., Kozubowski, J. A., Kapron, G., and Frontczak-Baniewicz, M., 2004, Serpentine-smectite interstratified minerals from Lower Silesia (SW Poland): Clays and Clay Minerals, v. 52, p. 55–65, doi: 10.1346/CCMN.2004.0520107.

Shutov, V. D., Drits, V. A., and Sakharov, B. A., 1969, On the mechanism of a postsedimentary transformation of montmorillonite into hydromica, *in* Heller, L., editor, International Clay Conference, Tokyo, Japan: Israel University Press, Jerusalem, p. 523–531.

Srodon, J., 1978, Correlation between coal and clay diagenesis in the Carboniferous of the upper Silesian coal basin, *in* Mortland, M. M., and Farmer, V. C., editors, Proceedings of the VI International Clay Conference, Oxford 10–14 July, 1978: Oxford, Elsevier, p. 251–260.

—— 1980, Precise identification of illite/smectite interstratifications by X-ray powder diffraction: Clays and Clay Minerals, v. 28, p. 401–411, doi:10.1346/CCMN.1980.0280601.

—— 1981, X-Ray identification of randomly interstratified illite-smectite in mixtures with discrete illite: Clay Minerals, v. 16, p. 297–304, doi:10.1180/claymin.1981.016.3.07.

—— 1984a, Mixed-layer illite-smectite in low-temperature diagenesis: Data from the Miocene of the Carpathian foredeep: Clay Minerals, v. 19, p. 205–215, doi:10.1180/claymin.1984.019.2.07

—— 1984b, X-ray powder diffraction of illitic materials: Clays and Clay Minerals, v. 32, p. 337–349, doi:10.1346/CCMN.1984.0320501.

—— 1999, Nature of mixed-layer clays and mechanisms of their formation and alteration: Annual Review of Earth and Planetary Sciences, v. 27, p. 19–53, doi:10.1146/annurev.earth.27.1.19

Srodon, J., and Eberl, D. D., 1984, Illite, *in* Bailey, S. W., editor, Micas: Washington D.C., Mineralogical Society of America, Reviews in Mineralogy, v. 13, p. 495–544.

Srodon, J., Eberl, D. D., and Drits, V. A., 2000, Evolution of fundamental-particle size during illitization of smectite and implications for reaction mechanism: Clays and Clay Minerals, v. 48, p. 446–458, doi: 10.1346/CCMN.2000.0480405.

Sucha, V., Kraus, I., Gerthofferova, H., Petes, J., and Serekova, M., 1993, Smectite to illite conversion in bentonites and shales of the East Slovak basin: Clay Minerals, v. 28, p. 243–253, doi:10.1180/claymin.1993.028.2.06.

Sudo, T., and Shimoda, S., 1977, Interstratified clay minerals—Mode of occurrence and origin: Minerals Science and Engineering, v. 9, p. 3–24.

Velde, B., and Brusewitz, A. M., 1982, Metasomatic and non-metasomatic low grade metamorphism of Ordovician meta-bentonites in Sweden: Geochimica et Cosmochimica Acta, v. 46, p. 447–452, doi: 10.1016/0016-7037(82)90235-6.

—— 1986, Compositional variation in component layers in natural illite/smectite: Clays and Clay Minerals, v. 34, p. 651–657, doi:10.1346/CCMN.1986.0340605.

Velde, B., and Espitalié, J., 1989, Comparison of kerogen maturation and illite/smectite composition in diagenesis: Journal of Petroleum Geology, v. 12, p. 103–110, doi:10.1111/j.1747-5457.1989.tb00223.x.

Velde, B., and Iijima, A., 1988, Comparison of clay and zeolite mineral occurrences in Neogene age sediments from several deep wells: Clays and Clay Minerals, v. 36, p. 337–342, doi:10.1346/CCMN.1988.0360407.

Velde, B., and Vasseur, G., 1992, Estimation of the diagenetic smectite to illite transformation in time-temperature space: American Mineralogist, v. 77, p. 967–976.

Velde, B., Suzuki, T., and Nicot, E., 1986, Pressure-Temperature-Composition of illite/smectite mixed-layer minerals: Niger delta mudstones and other examples: Clays and Clay Minerals, v. 34, p. 435–441, doi:10.1346/CCMN.1986.0340410.

Watanabe, T., 1981, Identification of illite/montmorillonite interstratification by X-ray powder diffraction: Journal of the Mineralogical Society of Japan, Special Issue v. 15, p. 32–41.

—— 1988, The structural model of illite/smectite interstratified mineral and the diagram for their identification: Clay Science, v. 7, p. 97–114.

Weaver, C. E., 1957, The clay petrology of sediments: Clays and Clay Minerals, v. 6, p. 154–187.

—— 1959, Possible uses of clay minerals in the search for oil: Clays and Clay Minerals, v. 8, p. 214–227.

Whitney, G., 1990, Role of water in the smectite-to-illite reaction: Clays and Clay Minerals, v. 38, p. 343–350.

Whitney, G., and Northrop, H. R., 1988, Experimental investigation of the smectite to illite reaction: Dual reaction mechanisms and oxygen-isotope systematics: American Mineralogist, v. 73, p. 77–90.